Photon-counting CT: Technical Principles and Clinical Prospects

Martin J. Willemink, MD, PhD • Mats Persson, PhD • Amir Pourmorteza, PhD • Norbert J. Pelc, ScD • Dominik Fleischmann, MD

From the Department of Radiology (M.J.W., M.P., N.J.P., D.F.) and Stanford Cardiovascular Institute (D.F.), Stanford University School of Medicine, 300 Pasteur Dr, S-072, Stanford, CA 94305-5105; Department of Radiology, University Medical Center Utrecht, Utrecht, the Netherlands (M.J.W.); Departments of Bioengineering (M.P., N.J.P.) and Electrical Engineering (N.J.P.), Stanford University, Stanford, Calif; Department of Radiology and Department of Imaging Sciences and Biomedical Informatics, Emory University School of Medicine, Atlanta, Ga (A.P.). Received November 15, 2017; revision requested January 2, 2018; final revision received January 23; accepted February 5. **Address correspondence to** M.J.W. (e-mail: *m.j.willemink@stanford.edu*).

Conflicts of interest are listed at the end of this article.

Radiology 2018; 289:293–312 • https://doi.org/10.1148/radiol.2018172656 • Content code: CT

Photon-counting CT is an emerging technology with the potential to dramatically change clinical CT. Photon-counting CT uses new energy-resolving x-ray detectors, with mechanisms that differ substantially from those of conventional energy-integrating detectors. Photon-counting CT detectors count the number of incoming photons and measure photon energy. This technique results in higher contrast-to-noise ratio, improved spatial resolution, and optimized spectral imaging. Photon-counting CT can reduce radiation exposure, reconstruct images at a higher resolution, correct beam-hardening artifacts, optimize the use of contrast agents, and create opportunities for quantitative imaging relative to current CT technology. In this review, the authors will explain the technical principles of photon-counting CT in nonmathematical terms for radiologists and clinicians. Following a general overview of the current status of photon-counting CT, they will explain potential clinical applications of this technology.

Since its introduction in the early 1970s, CT technology has undergone numerous advances, from single-section CT scanners to multidetector systems capable of covering the entire heart in a single rotation. In addition to improvements in rotation time and detector size, advanced reconstruction algorithms have also become available. Moreover, clinical CT scans can now acquire images at two energies, creating new opportunities for use in clinical practice.

Despite its remarkable success, CT technology still has substantial limitations. First, the exposure of patients to ionizing radiation remains a concern. Although radiation doses can be reduced, dose reduction causes other problems in CT images, such as image noise and distortions (known as artifacts). Second, CT has a limited ability to reliably help differentiate between pathologic and healthy tissues because of the low inherent contrast between different types of soft tissues. In clinical imaging, this is addressed with the administration of contrast agents. However, that brings up a third limitation: Iodinated contrast agents used in CT can cause kidney damage and can trigger allergic reactions (1). Last, x-ray attenuation values in CT images are expressed in Hounsfield units, which are influenced by factors such as tube voltage and surrounding anatomy. Consequently, voxel values in CT images may not represent actual tissue densities or contrast agent concentrations and can be ambiguous. This limitation can theoretically be solved with use of dual-energy CT (2), a technique that provides tissue-specific images and iodine concentration maps, resulting in CT images with absolute quantitative meaning. However, the separation between high- and low-energy photons (spectral separation) is suboptimal in current dual-energy CT scanners (3). The acquisition of CT images at more than two energy bins enables better tissue discrimination.

To help clinicians fully benefit from the possibilities of CT imaging, it is important that radiologists and clinicians grasp the principles of recent and upcoming advances, especially with promising but complex new techniques such as photon-counting CT on the horizon, ready to dramatically change CT. This technique has the potential to address several limitations of current CT technology. The goal of this review is to explain the technical principles of photon-counting CT in nonmathematical terms for radiologists and clinicians. An overview of the current status of photon-counting CT technology is followed by a discussion of potential clinical applications.

Physical Principles

Conflicts of Interest

None of the authors are industry employees. One author (M.P.) is a stockholder and consultant for Prismatic Sensors, a commercial spin-off from KTH Royal Institute of Technology in Stockholm, Sweden. One author (N.J.P.) is on the scientific advisory board of the same spin-off, Prismatic Sensors. Furthermore, he received research support from Philips Healthcare and GE Healthcare. However, for this project none of the authors received financial or research support from the industry and the current project itself also was not funded. Data and information were controlled by authors without conflicts of interest.

Energy-integrating and Photon-counting Detectors

Clinical CT scanners currently use energy-integrating detectors (EIDs). A detector bank typically consists of several rows of approximately 900 detector elements per row, separated by thin septa. Each detector element mea-

Abbreviations

CNR = contrast-to-noise ratio, EID = energy-integrating detector, PCD = photon-counting detector

Summary

Compared with current CT technology, photon-counting CT will allow for reduced radiation exposure, increased spatial resolution, correction of beam-hardening artifacts, and alternative contrast agent protocols while creating opportunities for quantitative imaging.

Essentials

- Photon-counting CT is a promising technique, with the potential to dramatically alter the clinical use of CT in the upcoming decades.
- New energy-resolving detectors enable detection of individual x-ray photons and measurement of their energy.
- Relative to conventional energy-integrating detector CT, photon-counting CT will allow for radiation dose reduction, increased spatial resolution, correction of beam-hardening artifacts, and use of alternative contrast agents while creating opportunities for quantitative imaging.

sures the total x-ray energy deposited in the detector during each measurement interval. Their operating principle is illustrated in Figure 1, *A*. Incident x-rays are absorbed in the upper layer, which is a scintillator made of a material that converts x-rays into visible light. When x-ray photons strike the scintillator, a shower of secondary visible light photons is generated. These are absorbed by a photodiode made of a semiconducting material, which measures the amount of incident light and generates an electrical signal proportional to the total energy deposited during a measurement interval, rather than the energy of an individual x-ray photon.

Photon-counting detectors (PCDs), on the other hand (Fig 1, *B*), do not require a separate layer to convert x-rays into light but consist of a single thick layer (1.6–30 mm depending on material [4,5]) of a semiconductor diode, on which a large voltage is applied. If an incident x-ray is absorbed in the semiconductor, it generates a cloud of positive and negative charges (6) pulled away from each other rapidly. The moving charges generate an electrical pulse in the wires attached to the electrodes, which is registered with an electronic readout circuit. PCDs thus convert individual x-ray photons directly into an electric signal, unlike EIDs as used in current CT, which require the additional step of converting photons to visible light.

The electrical signal generated by an individual detector element in a PCD is illustrated in Figure 2. Each photon that hits the detector element generates an electrical pulse with a height proportional to the energy deposited by the photon. The electronics system of the detector counts the number of pulses with heights that exceed the preset threshold level. The threshold is set at levels that are higher than the electronic noise level but lower than pulses generated by incoming photons. Furthermore, by comparing every pulse to several threshold levels, the detector can sort the incoming photons into a number of energy bins (typically two to eight), depending on their energy (Fig 3). Thus, electronic noise is effectively excluded from photon and/or pulse counts (although electronic noise still affects the pulse height and, therefore, the measured photon energy). EIDs, on the other hand, measure and integrate the total energy deposited during the measurement interval, including electronic noise. This corresponds to the total area under the signal curve in Figure 2 and gives less detailed information compared with PCDs.

Current Challenges

In the previous section, we have described an ideal PCD. To understand why photon-counting CT systems are not yet clinically available, it is important to grasp why a real-world PCD may not attain the performance of an ideal one and identify the technical challenges that we must overcome. The effects causing performance degradation are dependent on the type of sensor material used in detectors. Research on PCDs has focused on cadmium telluride, cadmium zinc telluride, and silicon (6).

Cross talk.—In an ideal PCD, a photon creates a signal only in the detector element on which it impinges. In reality, there are several physical effects that may cause a single photon to be registered as a count event in more than one detector element. In a silicon detector, a large proportion of the photons interact by Compton scattering in the detector material, depositing a small fraction of their energy in the detector element. The scattered photon then moves on in a new, random direction, possibly depositing its remaining energy in another detector element (7). With cadmium telluride and cadmium zinc telluride, the probability of Compton scatter is low. However, part of the energy deposited in the original interaction may be released in the form of a fluorescent x-ray, which can be absorbed in a neighboring detector element, as shown in Figure 4, *A* (8,9). Although Compton scattering and x-ray fluorescence are different physical effects, they both cause photons to be registered with incorrect energy ranges and possibly be counted more than once.

In both silicon and cadmium telluride or cadmium zinc telluride detectors, cross talk between detector elements can also be attributed to an effect called charge sharing. As shown in Figure 4, *B*, each absorbed x-ray photon generates clouds of positive and negative charges in the sensor material. If the photon is absorbed close to the border between two detector elements, part of the charge cloud may extend into a neighboring detector element, which can register part of the photon energy. The result is that the photon is counted twice, both in the detector element of incidence and in a neighboring detector element, with part of the original energy registered in each (8).

The various kinds of cross talk degrade image quality in several ways. First, they deteriorate spatial resolution (ie, blur the image) by causing photons to be registered in the wrong detector element (9). Second, they may lead to a photon being counted more than once. This decreases the image contrast-to-noise ratio (CNR), as all effects that introduce extra randomness in the number of counted photons produce extra image noise (10,11). Third, the different forms of cross talk degrade the energy resolution of the detector, reducing the reliability of the energy information and causing increased image noise in material-selective images (9,12).

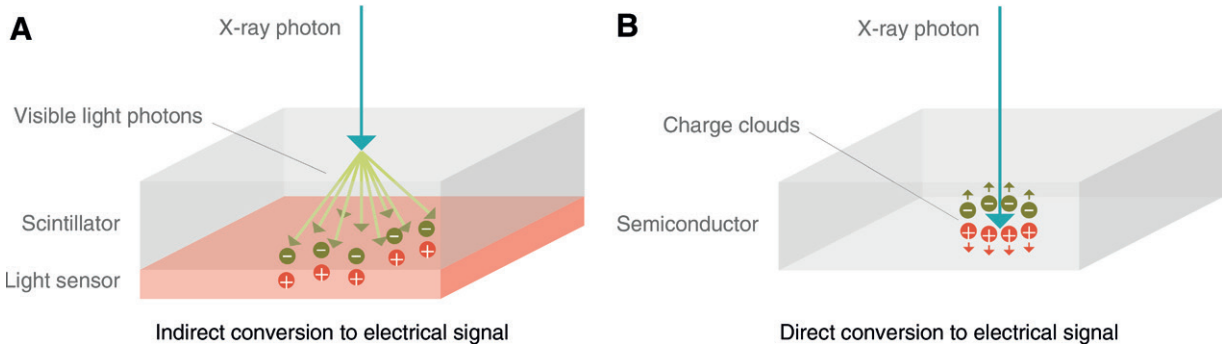

Figure 1: Diagrams show detector types. *A*, In conventional energy-integrating detector, an incident x-ray photon is converted into a shower of visible light photons in a scintillator. Visible light hits an underlying light sensor, where it generates positive and negative electrical charges. *B*, In photon-counting detector, the x-ray photon is absorbed in a semiconductor material, where it generates positive and negative charges. Under the influence of a strong electric field, the positive and negative charges are pulled in opposite directions, generating an electrical signal.

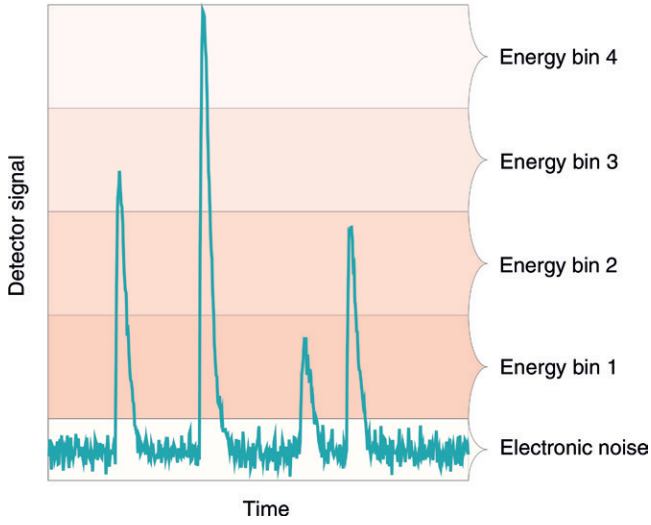

Figure 2: Diagram illustrates operating principle of a photon-counting detector. Each registered photon gives rise to an electrical pulse in the detector readout electronics, with the height of each pulse proportional to the individual photon energy. The detector counts the number of pulses with a height larger than a preset threshold, thereby eliminating electronic noise. By setting more than one threshold, the registered photons can be sorted into several energy bins on the basis of their energy range.

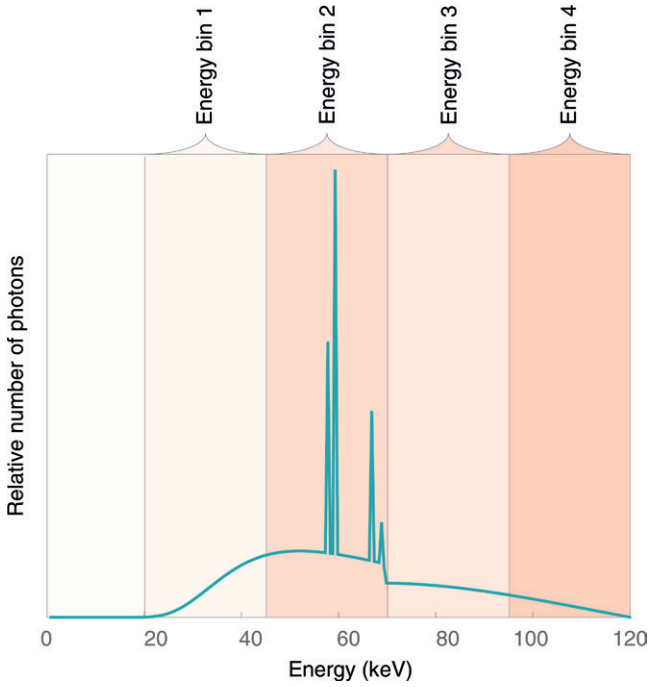

Figure 3: In an energy-resolving photon-counting detector, the measured x-ray spectrum is divided into a number of energy bins. In a real detector, the bin edges are not perfectly sharp as in this idealized illustration. Some degree of overlap between the energy bins is expected.

Pile-up.—A fast detector is required to count individual photons. Up to several hundred million photons impinge on the detector per second per square millimeter (5), and the sensor material must therefore be able to transport the released charges rapidly and the readout electronics must be able to count the resulting pulses fast enough. The need for sufficiently fast and stable detectors is one of the reasons why photon-counting CT scanners are only recently becoming available to be used at clinical CT dose levels (13). However, PCDs are widely used in PET, SPECT, and dual-energy x-ray absorptiometry and have been introduced in one commercial mammography system (MicroDose; Philips Healthcare, Best, the Netherlands), where the count rates are substantially lower. If the photons arrive too fast, some of the resulting electrical pulses will superimpose on each other, a phenomenon called pulse pile-up (Fig 5, *A*). If two consecutive pulses are almost simultaneous, they will be registered as a single pulse with an energy equal to the sum of the energies of the two incident photons. If the difference in arrival times between pulses is slightly larger, the detector may be able to register them as two separate counts but the partial overlap can still cause an error in the measured photon energy (Fig 5, *B*).

Pile-up has two effects on image quality. First, the count loss increases image noise because fewer photons contribute to the measurement (14). Second, the energy resolution deteriorates, with similar effects to cross talk (14–16). Because pile-up occurs for high count rates, it does not degrade all parts of the image

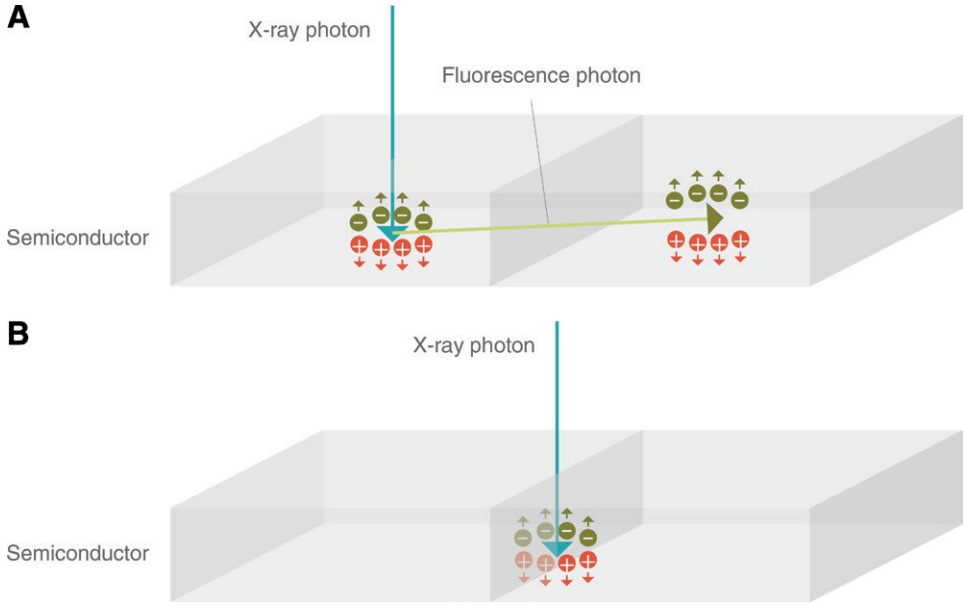

Figure 4: Different types of cross talk between detector elements. *A*, Diagram shows fluorescence cross talk. X-ray photon only deposits part of its energy in detector element where it is incident. The rest of the energy is carried away by a fluorescence photon, which generates charges in another random location, possibly in another detector element. Compton scattering has a similar effect. *B*, Diagram shows charge-sharing cross talk. When an incident x-ray photon is absorbed on the border between two detector elements, part of the generated charges are registered in each of the two detector elements. Both cross talk and charge sharing can cause part of the photon energy to be registered in the wrong detector element, which degrades image quality.

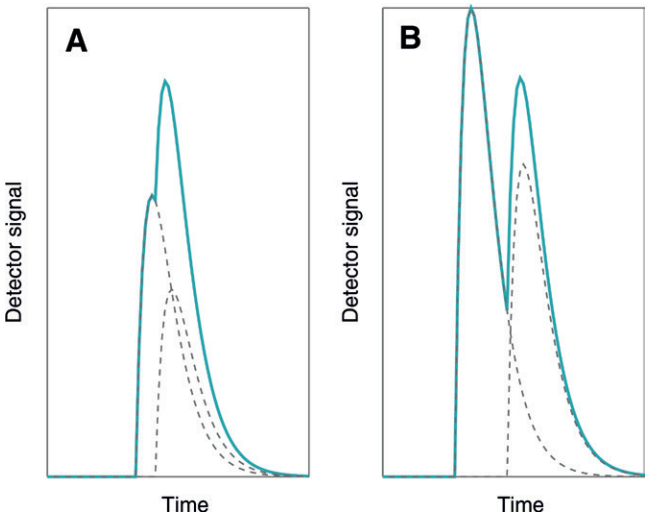

Figure 5: Diagrams illustrate pulse pile-up. *A*, If two photons arrive very closely spaced in time, the detector is not able to separate the pulses generated by each photon (dashed lines) and registers them as a single count (solid line). *B*, If the difference in arrival times between the photons is slightly larger, they may be registered as two separate counts, but with an error in the registered energy.

equally but is concentrated in low-attenuation regions, such as near the skin and in the lungs. These effects can be minimized by designing smaller detector elements and faster counters. However, there is a tradeoff between pile-up and charge sharing as detector elements become smaller.

Figure 6 shows two idealized behaviors of PCDs as a function of incident count rate (15,17): a nonparalyzable detector, for which the registered count rate increases toward a limiting maximum value, and a paralyzable detector, for which the registered count rate increases, reaches a maximum, and then decreases again. A real PCD may exhibit one or the other, or some hybrid behavior.

Noise Reduction and CNR Improvement

An ideal PCD can produce images with lower image noise than an ideal EID because of the way photons with different energies are weighted. Because an EID measures the total absorbed x-ray energy, high-energy photons contribute relatively more to the total signal than do low-energy photons. However, this weighting does not result in optimal CNR because the tissue contrast is low at high energies.

To optimize CNR in the image, the largest weight may be assigned to photons with low energies, where the contrast between tissues is the highest, as shown in Figure 7. An energy-resolving PCD is able to assign higher weight factors to low-energy bins, resulting in improved CNR (4,18,19). A disadvantage of giving low-energy photons higher weight is the resultant increase in beam-hardening artifacts, as tissue attenuation in the low-energy part of the x-ray spectrum is more heterogeneous (20). This drawback can be eliminated with material decomposition, as described below. The benefits associated with the ability of a PCD to assign more weight to low-energy photons have been assessed in two clinical studies. Pourmorteza et al (21) reported up to 30% improvement in gray matter–white matter CNR in noncontrast PCD human brain scans, and Symons et al (22) have shown that PCD head and neck CT angiograms had 9% lower image noise compared with EID at a similar dose. A summary of the factors determining the performance of an ideal PCD is shown in Table 1.

In practice, neither EID nor PCD are ideal, and the exact performance of future commercial PCDs requires further investigation. However, prototype photon-counting CT scanners have been tested in the past few years and have shown substantial advantages. First, the benefit of optimal energy weighting is significant for imaging materials with high attenuation at low energies, such as calcium or iodine (4,22). Second, PCDs have a particular advantage over EIDs when used for low-dose imaging because they effectively eliminate electronic noise (Fig 2). At high x-ray intensities, the effect of electronic noise in EID is negligible. However, at low intensities, such as in low-dose imaging or behind structures with a high degree of attenuation (eg, bone or metal), electronic noise can degrade the image substantially

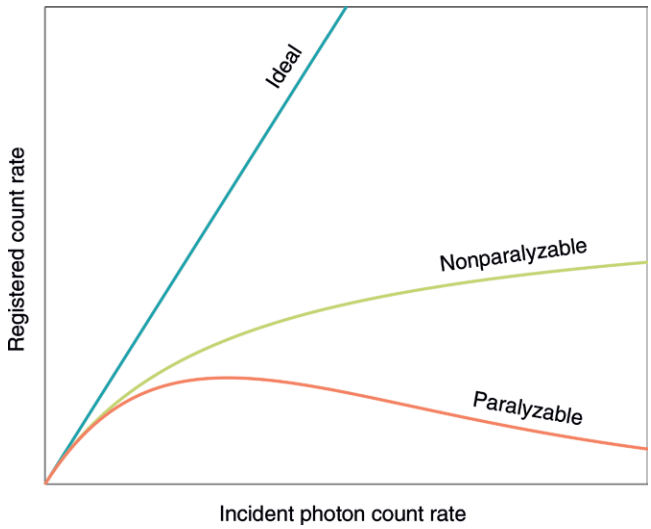

Figure 6: Examples of detector behavior under high-count-rate illumination. For an ideal detector, the registered count rate is equal to the incident count rate. A real-life detector follows the ideal curve for low count rates but starts to lose counts due to pile-up as fluence rate increases. Two models of detector behavior are plotted: a nonparalyzable detector, whose registered count rate increases slowly toward an asymptotic value, and a paralyzable detector, whose registered count rate reaches a peak value and then drops again.

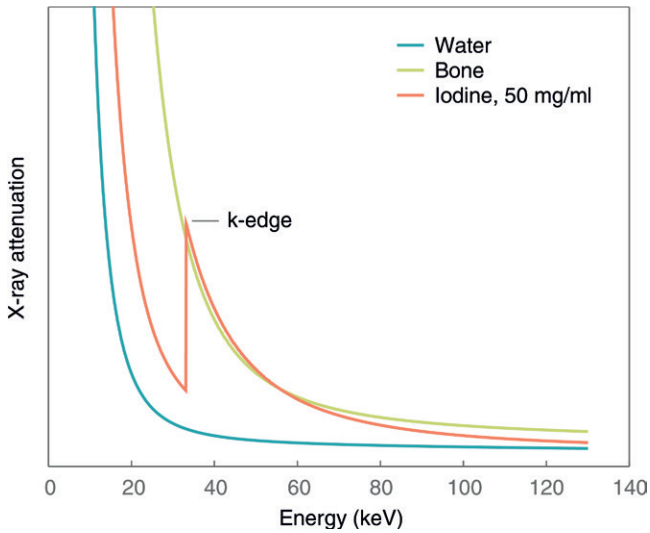

Figure 7: Graph shows attenuation coefficient as a function of energy for water, bone, and iodinated contrast agent (50 mg iodine per milliliter). The difference between the attenuation coefficients for different materials is largest for low energies. A heavy element such as iodine has a k-edge in the diagnostic energy range and can therefore be uniquely identified with an energy-resolving measurement.

(27). Thus, the dose efficiency decreases at low intensities for an EID but remains constant for a PCD (Fig 8). This effect has been investigated in lung phantoms (25) and in dose-reduced chest CT scans of humans (26,28) and showed up to 20% reduction in image noise.

Spatial Resolution

The spatial resolution achievable with any CT detector is primarily determined by its detector element size, which is close to 1 × 1 mm^2 for current systems. Because the x-ray beams diverge, the approximate resolution that can be achieved at the isocenter is obtained by dividing the size of the detector element by a geometric magnification factor, typically 1.5–2, giving a reconstructed image resolution close to 0.5 × 0.5 mm^2. The detector element size of EIDs has not significantly changed during the past 2 decades. This is because detector elements for EIDs must be separated from each other by thin, highly reflecting septa to avoid cross talk between secondary light photons generated in the scintillator. Small detector element areas make detectors increasingly difficult to manufacture. Moreover, the overall increase in the detector area covered by the optically isolating septa leads to decreased radiation dose efficiency. PCDs do not have separate scintillator elements and septa and can therefore be manufactured with smaller detector elements. In fact, PCDs must have smaller detector elements than EIDs to avoid pile-up because current detectors are not fast enough to resolve the individual photons unless the photon flux is split into submillimeter-sized detector elements. The detector element sizes most commonly considered for photon-counting CT range from 0.11 × 0.11 mm^2 to 0.5 × 0.5 mm^2 (Table 2), which together with the magnification factor give an image spatial resolution limit of 0.07 × 0.07 mm^2 to 0.28 × 0.28 mm^2 (5,30,33–36). Small detector element size may translate into improved visualization of fine detail and image noise reduction through anti-aliasing, particularly for high-spatial-resolution images (38,39). The main limitations of small detector element size are charge sharing and escape of fluorescence and scattered x-rays, which can cause a decrease in dose efficiency and compromise energy information (8,40). Nevertheless, the detector element sizes currently considered for photon-counting CT are quite small. Note that the image spatial resolution values given above are the theoretically achievable values if the x-ray tube focal spot is very small. In practice, the PCD detector element sizes will be small enough that the image resolution is mostly limited by blurring due to the x-ray tube focal spot. Improved x-ray tubes are therefore needed to fully benefit from the smaller detector elements.

Material Decomposition

There are two primary ways to use the energy information from spectral CT data (besides separate images of each energy bin): energy weighting and material decomposition. Energy weighting consists of assigning more weight to specific energy bins (18,19,41,42). The goal is to generate the best possible image quality for a given imaging scenario, for example, visualization of iodinated contrast material.

Material decomposition is achieved by determining the full energy dependence of the attenuation curve in every image voxel (2,34,43). Rather than measuring the x-ray attenuation in a very large number of energy bins, a small number of energy bins is sufficient for this purpose. This is explained by the finding that any material consisting of light elements, such as human tissue, is approximately equivalent to a combination of two basis materials, as far as x-ray attenuation properties are concerned (2). Although any pair of materials can be chosen as basis materials, herein we will

Table 1: Summary of Factors Determining the Performance of an Ideal Photon-counting Detector

Parameter	Feature Detection*	Material Quantification†
Higher geometric efficiency	1.5-fold improvement	1.5-fold improvement
Better spectral separation	Improved weighting (4,18,21,22); 1.3–2.5-fold improvement	Material decomposition (23,24); 2.0–3.1-fold improvement
No electronic noise	>1-fold improvement at very low count rate (25,26)	>1-fold improvement at very low count rate
Smaller detector elements	>1-fold improvement for high-spatial-resolution tasks	>1-fold improvement for high-spatial-resolution tasks
Total	2.0–3.8-fold improvement or more	3.0–4.6-fold improvement or more

Note.—Data are upper limits to the performance achievable with a photon-counting detector in practice, compared to an energy-integrating detector and to dual-source CT available today. Numbers in parentheses are references. The higher geometric efficiency comes from the possibility of removing the separators between detector elements (assumed here to be 0.2 mm thick in a 1.1 × 1.1 mm^2 detector element). In a real detector, however, an antiscatter grid is likely needed to reduce the amount of scatter from the patient. The benefit from the absence of electronic noise and from the smaller detector elements are strongly dependent on the task, so no numbers are given.

* Gray-scale imaging. Energy-integrating single-energy CT = 1.0.

† Spectral imaging. Dual-source dual-energy CT = 1.0.

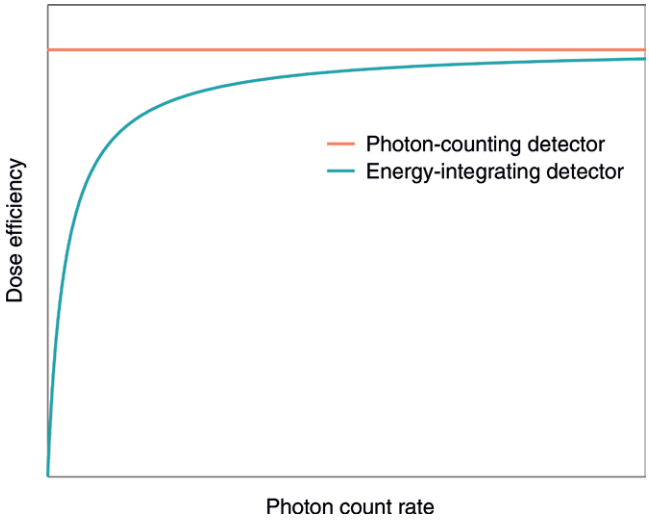

Figure 8: Graph illustrates dose efficiency for low count rates. A photon-counting detector has a constant dose efficiency as a function of count rate (except for very high count rates, where pile-up occurs). For an energy-integrating detector, the electronic noise becomes significant at very low count rates, reducing dose efficiency.

assume that these materials are water and calcium. Any human tissue can therefore be represented by a point in a diagram whose axes are the concentrations of the two basis materials, as shown in Figure 9, *A*. Although in reality human tissue is not composed of water and calcium, it has the same x-ray attenuation coefficient at all energies as the combination of these materials. Elements with high atomic numbers show a so-called k-edge, which is a step change in the attenuation at a specific x-ray energy (Fig 7). A k-edge in the x-ray attenuation curve identifies the corresponding element uniquely, so if a contrast agent containing a k-edge material is present, the concentration of that material is added to this diagram as a third dimension (Fig 9, *B*). Furthermore, the assumption that two basis materials suffice to represent all human tissues is an approximation, and ongoing research is investigating whether a material of low atomic number, for example, fat, could be added as an additional dimension in the diagram (44).

By performing material decomposition from a number of energy-selective images, a set of basis image maps is generated (Fig 10). Each map contains the equivalent concentration of one of the basis materials for each voxel in the image. These basis material images can be displayed directly to show the distribution of a certain material, such as a contrast agent. Alternatively, they may be processed to form virtual monochromatic images (22,23,45), virtual noncontrast images (46), or material-specific color-overlay images (47–49) (Figs 11–13). Because the full energy-dependent attenuation is considered, the resulting images can in theory be completely free of beam-hardening artifacts. Material decomposition thus eliminates the trade-off between beam hardening and CNR that affects energy-weighted images. It is also possible to generate virtual Hounsfield unit images (50), mimicking the CT numbers in images acquired with conventional CT, but without beam hardening, which can be another benefit of the clinical adoption of photon-counting CT.

To find the x-ray attenuation properties of a piece of tissue, the concentrations of water and calcium must be measured. Solving for two unknowns is possible with two or more equations, meaning that measurements at two energy bins, or three if a k-edge material is also present, are in principle sufficient to reconstruct a monochromatic image at any energy. However, increasing the number of energy measurements improves the precision to which each photon energy is measured and therefore gives lower image noise in the resulting material-specific or weighted images (24,51). Another benefit of using a larger number of energy measurements is to allow simultaneous quantification of more than one contrast agent.

One important application of material decomposition is to improve accuracy for measurement of the concentration of a contrast agent. The amount of contrast agent in an image voxel can be separated from the other constituents if three parameters are measured: the concentrations of water, calcium, and contrast agent. Solving for these three values requires measurements at three or more energy bins (43). Existing techniques for measuring iodine concentration with two energies (eg,

Table 2: Current Photon-counting CT Projects Targeted Toward Full-Body Clinical CT

Project	Detector Material*	Detector Element Size (mm^2)†	Current Status	Reference
GE Healthcare (Chicago, Ill)/Stanford University (Stanford, Calif)/Rensselaer Polytechnic Institute (Troy, NY) high-dose efficiency CT	CZT, planned integration with dynamic bowtie	0.5 × 0.5	Table-top system under construction at Rensselaer Polytechnic Institute	29
Medipix All Resolution System (MARS Bioimaging, Christchurch, New Zealand)	CZT	0.11 × 0.11	Imaging of specimens and small animals. Human-size scanner under construction.	30
Philips Healthcare (Best, the Netherlands) spectral photon-counting CT	CZT	0.5 × 0.5	Imaging of specimens and small animals. Prototype system with small detector installed in human-sized gantry in Lyon, France.	31,32
KTH Royal Institute of Technology (Stockholm, Sweden)/Prismatic Sensors (Stockholm, Sweden) silicon strip	Silicon	0.5 × 0.4	Table-top measurements at KTH Royal Institute of Technology	5
Siemens (Forchheim, Germany) dual detector	Dual-source CT with one CdTe photon-counting detector	0.225 × 0.225, detector elements binned into macro mode (0.9 × 0.9) and sharp mode (0.45 × 0.45)	Prototype human-size systems installed at Mayo Clinic (Rochester, Minn), at National Institutes of Health (Bethesda, Md), and in Forchheim, Germany. Research imaging of human volunteers	33

* CdTe = cadmium telluride, CZT = cadmium zinc telluride.

† Detector element sizes are the actual physical sizes, that is, not rescaled to isocenter.

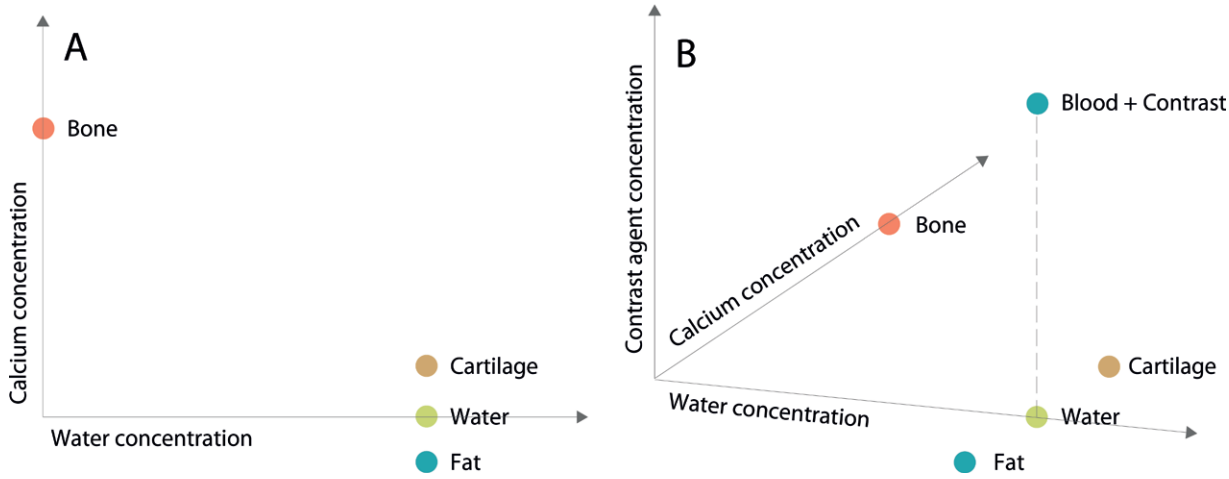

Figure 9: Material decomposition. *A*, The x-ray attenuation properties of any material in the human body correspond to one point in a two-dimensional diagram with water and calcium concentrations on the axes. *B*, If a k-edge contrast agent such as iodine or gadolinium is present, it is added as a third dimension to the diagram. The contrast agent concentration can thus be measured separately from the calcium and water concentrations.

dual-energy CT) therefore must build on assumptions about the tissue composition (52). If these assumptions are wrong, for example, if there is calcium in the same voxel, the measurement will be inaccurate (53). Photon-counting CT will likely allow more accurate measurement of iodine concentrations (23). However, because its k-edge at 33 keV is the distinguishing feature of the iodine attenuation curve, independent quantification of iodine requires that some photons be transmitted at those low energies. Although this is realistic for tissue with a small cross-section diameter, such as in children (12,54), contrast media with higher atomic number and higher k-edge energies, such as gadolinium or targeted nanoparticles, may be better suited for performing imaging studies in large patients (12,48,49,55).

Current Status

Although clinical photon-counting CT scanners are not yet commercially available, several groups and manufacturers

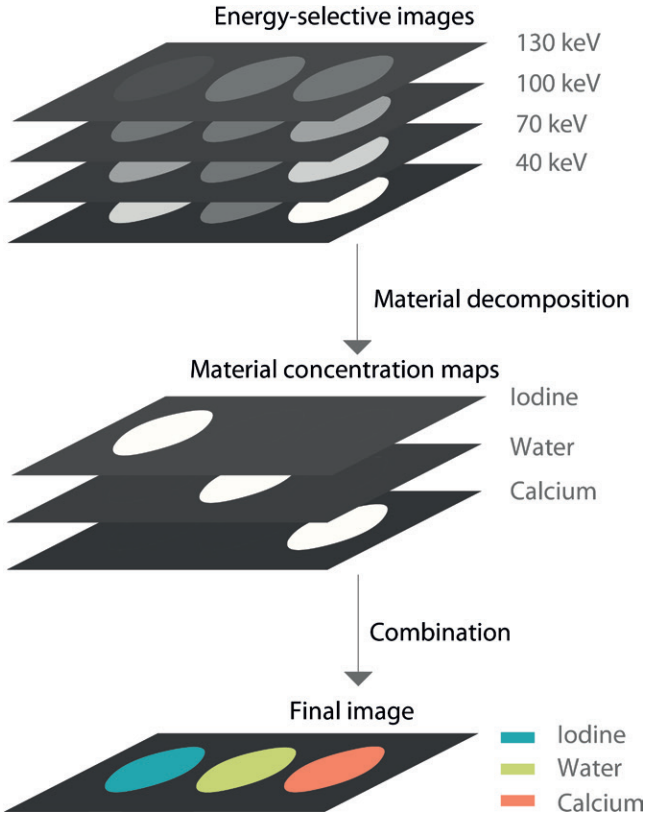

Figure 10: Material decomposition. Energy-selective images are generated from the number of registered counts in each energy bin. From these images, a set of material concentration maps is generated through a data-processing method known as material decomposition. Material concentration maps can then be combined in different ways to form the final image that is shown to the radiologist. This image can, for example, be a color-coded map showing different materials, a virtual monochromatic image, or a virtual noncontrast image.

are developing full-body photon-counting CT systems, and these are in various stages of completion. An overview of the development efforts known to the authors is presented in Table 2.

Clinical Applications

Although prototype photon-counting CT scanners for humans have been developed, these are intended for research use. Prototype photon-counting CT scanners allow manufacturers to gather data to optimize and design an eventual clinically applicable device. Further, mass production of PCDs for medical use for CT does not yet exist. Industrialization of detector production is necessary to achieve device costs that are acceptable to the medical community. Considering the current stage of development, a reasonable expectation is that photon-counting CT scanners will be introduced in clinical practice within 5–10 years. On the basis of published experience with prototype systems, simulation studies, and theoretical possibilities, photon-counting CT will likely allow for substantial radiation dose reductions, improved spatial resolution, a decrease in artifacts, and the possibility of using other contrast agents and reduced iodine concentrations while possibly expanding opportunities for quantitative imaging.

Radiation Dose

During the past decade, the number of CT examinations increased yearly, with a 6.5% increase in the United States, resulting in a total of approximately 80 million CT scans per year (56,57). Despite the introduction of several dose-reducing techniques, such as iterative reconstruction, automatic exposure control, and electrocardiography-triggered imaging, radiation exposure remains a concern (58–60).

Image noise levels with photon-counting CT will be lower at the same level of x-ray exposure compared with conventional CT scanners because PCDs minimize electronic noise and enable optimal x-ray photon energy weighting (Fig 14). This can be used to reduce radiation doses. Kappler and colleagues (61) evaluated contrast and image noise by using water phantoms. They found increased iodine contrast with similar image noise compared with EID, resulting in a radiation dose reduction of up to 32%. Recent in vivo human experiments confirmed a dose reduction of up to 34% in photon-counting CT scans of the chest and brain (21,26).

Giersch et al (41) assessed the possibilities of energy weighting by simulating an ideal system. They found that images could be acquired with the same image quality using fewer photons, resulting in a radiation dose reduction by a factor of 2.5 (60% reduction). Photon-counting CT has the potential to improve CNR, which could be clinically used to reduce either the amount of contrast agent or the radiation dose (4,6,22). Compared with conventional CT, the smaller detector element size in photon-counting CT can be used for two different types of improvement, either increasing spatial resolution at a similar radiation dose and noise level or lowering radiation dose at a similar spatial resolution and noise level. This is because decreasing the detector element size means acquiring more data points. Even though this gives more noise in each individual detector element, the net result is that more high-spatial resolution information is obtained, which the reconstruction algorithm can translate to lower noise in the final images (38). A recent in vivo human study has shown that additional dose reduction of up to 36% is achievable with high-spatial-resolution photon-counting CT (39). Thus, it is likely that photon-counting CT will reduce radiation levels by approximately 30%–60%, depending on the imaging task.

Spatial Resolution

PCDs enable improved spatial resolution compared with conventional EIDs. Higher spatial resolution may be beneficial for multiple clinical applications in which small anatomic and pathologic structures require evaluation and to reduce "blooming," as discussed below.

Breast CT.—Currently, PCDs are being used on an experimental basis in dedicated breast CT systems (62,63). High spatial resolution is an advantage in breast imaging, which must depict small features and subtle lesions. PCDs are a viable option for dedicated cone-beam CT of the breast, considering the small size relative to whole body imaging, relatively homogeneous tissue content, and lack of motion. Low x-ray photon-count rate detectors can therefore be used in breast imaging. For most other clinical applications, fast PCDs are necessary.

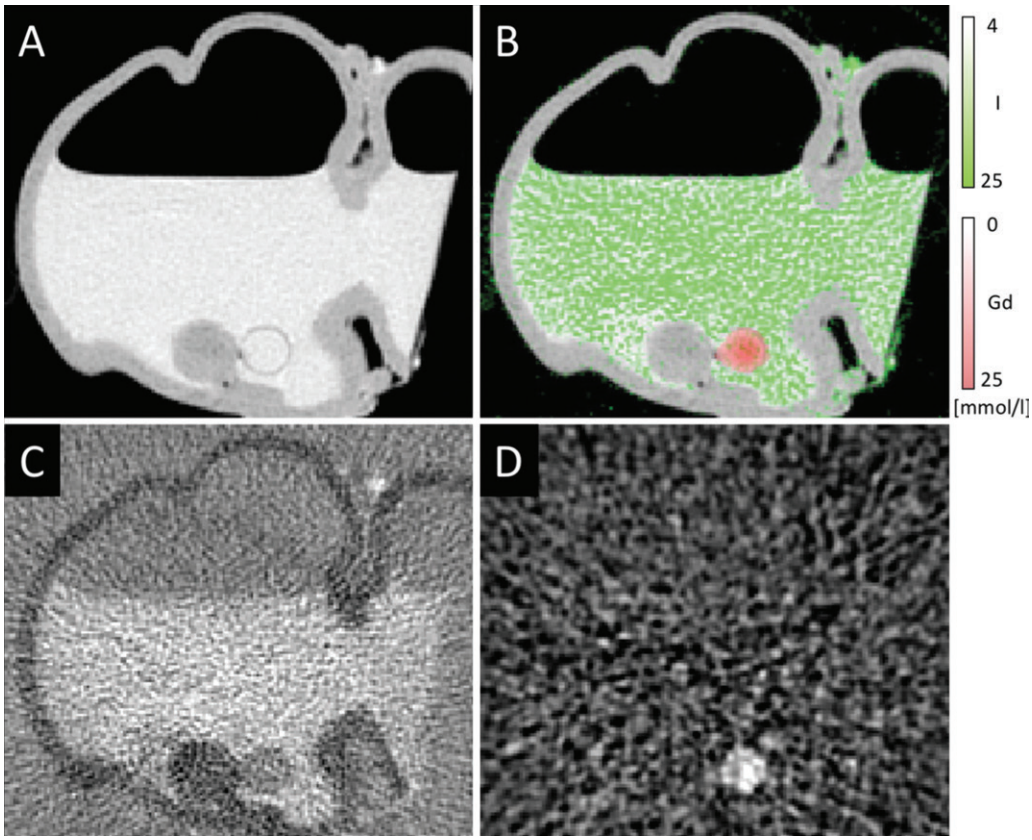

Figure 11: Colon phantom images obtained with a photon-counting CT prototype (Philips Healthcare, Best, the Netherlands). *A*, Conventional CT scan (window width, −300 HU; window level, 1000 HU). *B*, Conventional CT scan (image in *A*) with overlay of iodine (green) and gadolinium (red). *C*, Iodine image (window width, 0 mmol/L; window level, 80 mmol/L). *D*, Gadolinium image (window width, 5 mmol/L; window level, 20 mmol/L). Both material images (*C* and *D*) are generated from decomposition algorithm and are visually and quantitatively distinguishable. Therefore, this procedure enables a separation between gadolinium-enhanced polyp tissue and iodine-tagged fluids and feces in colon. (Image courtesy of Peter B. Noël, PhD, Technical University of Munich, Germany, and reprinted, with permission, from reference 31.)

Temporal bone CT.—Recent advances in fast PCDs have made whole-body photon-counting CT possible, resulting in a variety of clinical applications. High spatial resolution is essential to the imaging of the temporal bone. Small structures such as the auditory ossicles are inadequately depicted on low-resolution images. Leng and colleagues (64) used a research full-body photon-counting CT system to scan the cadaveric temporal bone of a swine at a high spatial resolution. Photon-counting CT allowed for clear visualization of crucial anatomic structures, such as the stapes superstructure, while reducing the radiation dose compared with high-spatial-resolution EID, which uses a removable comb that blocks up to three-quarters of the incident photons.

Chest CT.—Leng et al (37) evaluated another frequently used clinical protocol, high-spatial-resolution chest CT. The authors scanned an anthropomorphic lung phantom and a cadaveric swine lung using both photon-counting CT and conventional CT and found improved image quality with photon-counting CT. In another study (65), they showed that shape and texture information improved with photon-counting CT for both lung nodules and kidney stones owing to higher spatial resolution, but also found that image noise increased. The same group evaluated a set of synthetic lung nodules in the study by Zhou et al (66). The lung nodules, which had different shapes, sizes, and densities, were scanned by using high-spatial-resolution photon-counting CT and conventional CT. The authors concluded that high-spatial-resolution photon-counting CT allowed for improved lung nodule characterization (regarding volume and shape) compared with conventional CT.

Cardiovascular CT.—CT angiography has replaced diagnostic catheter angiography in all vascular territories, except for those where spatial resolution is insufficient. Electrocardiography synchronization and faster gantry rotation times have improved the temporal resolution of CT to such a degree that coronary CT has become an established technique for several indications (67). CT is well-suited to rule out coronary artery disease in relatively large normal vessels, but its specificity remains low. This is to be expected, as gauging the degree of stenosis requires much higher spatial resolution to identify vessel lumen borders within a fraction of a millimeter. Furthermore, calcified plaque is often blamed for "blooming" and obscuring the interface between flow channel and vessel wall. However, blooming simply represents the point-spread

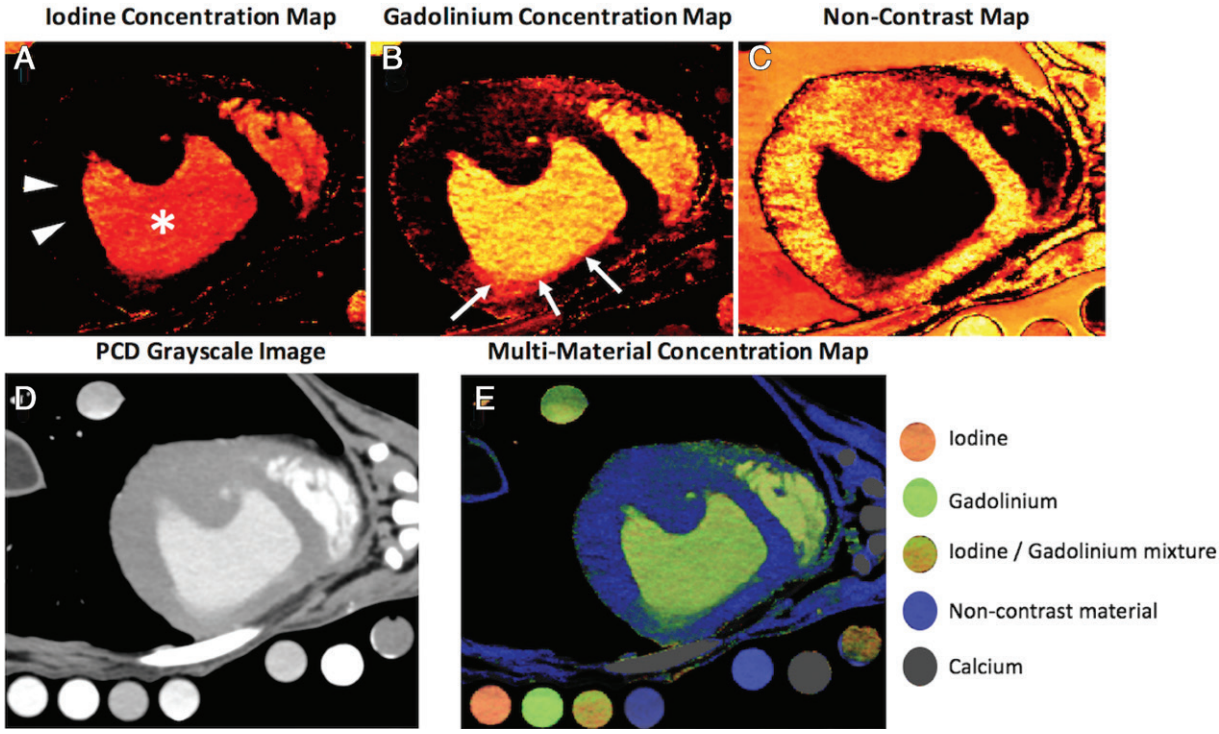

Figure 12: Sample results of multi k-edge material decomposition of photon-counting detector (PCD) CT images of canine heart. *A*, Iodine concentration, *B*, gadolinium concentration, and, *C*, noncontrast maps. Iodine material map shows first-pass enhancement of blood pool, whereas gadolinium map shows late enhancement of subendocardial scar tissue (arrows). *D*, Conventional single-energy image with PCD CT. *E*, Multimaterial concentration map obtained by combining the material maps shows that differentiation between infarcted myocardium (arrows in *B*), remote myocardium (arrowheads in *A*), and left ventricle blood pool (∗ in *A*) is possible with high contrast-to-noise ratio compared with conventional single-energy image. (Reprinted, with permission, from reference 48.)

function of the scanner, that is, its spatial resolution, disclosed by a high-contrast interface. Thus, it is conceivable that improved spatial resolution may increase specificity. Figures 15–17 show the ultra-high-spatial-resolution capabilities of a prototype photon-counting CT system compared with standard resolution.

Currently, the gantry rotation time of the prototype scanners has been limited to a maximum of 0.5 second, mainly due to data transfer rate limitations and the prototype nature of the scanners and the fact that some of the additional PCD-specific gantry parts may not have been tested for higher rotation speeds at this point. However, we expect that a commercial photon-counting CT scanner would have a temporal resolution no less than that of the state-of-the-art EID scanners.

Several other vascular territories may also benefit from the availability of photon-counting CT scanners. Critical lower limb ischemia and below-knee arterial calcification are currently inadequately assessed with CT angiography, mainly due to insufficient spatial resolution. Small-vessel vasculitis with subtle luminal changes and fibromuscular dysplasia—currently assessed with intraarterial angiography and pressure measurements—may become indications for CT as well if spatial resolution is improved. Figure 16 shows a carotid plaque cast acquired with conventional CT and a prototype photon-counting CT system.

Orthopedic trauma CT.—High-density structures such as the skeleton can be visualized excellently with CT. However, visualization of complex fractures of small bones (eg, of the wrist) can potentially be improved by using high-spatial-resolution photon-counting CT. Moreover, material decomposition can be used to reconstruct images without calcium (virtual noncalcium images), allowing for evaluation of bone marrow edema without the need for MRI. Bone marrow edema assessment has been evaluated with dual-energy CT by multiple groups (70–73) and is expected to improve with photon-counting CT. However, to our knowledge, evaluation with photon-counting CT systems is yet to be performed.

Head and neck CT.—For tumor staging of laryngeal and hypopharyngeal cancer, it is essential to differentiate tumors that invade the laryngeal cartilages from those that do not. CT is used for the detection of cartilage invasion; minimal amounts of contrast agent can be found in the cartilage when invasion is present. However, the density of nonossified laryngeal cartilage is similar to that of tumors with conventional CT, making them almost indistinguishable (74). Higher spatial resolution and material differentiation by using photon-counting CT may allow for improved detection of cartilage invasion, leading to improved tumor staging of these types of cancer.

Artifacts

Beam-hardening artifacts.—Gray-scale PCD images are more susceptible to beam-hardening artifacts than are conventional

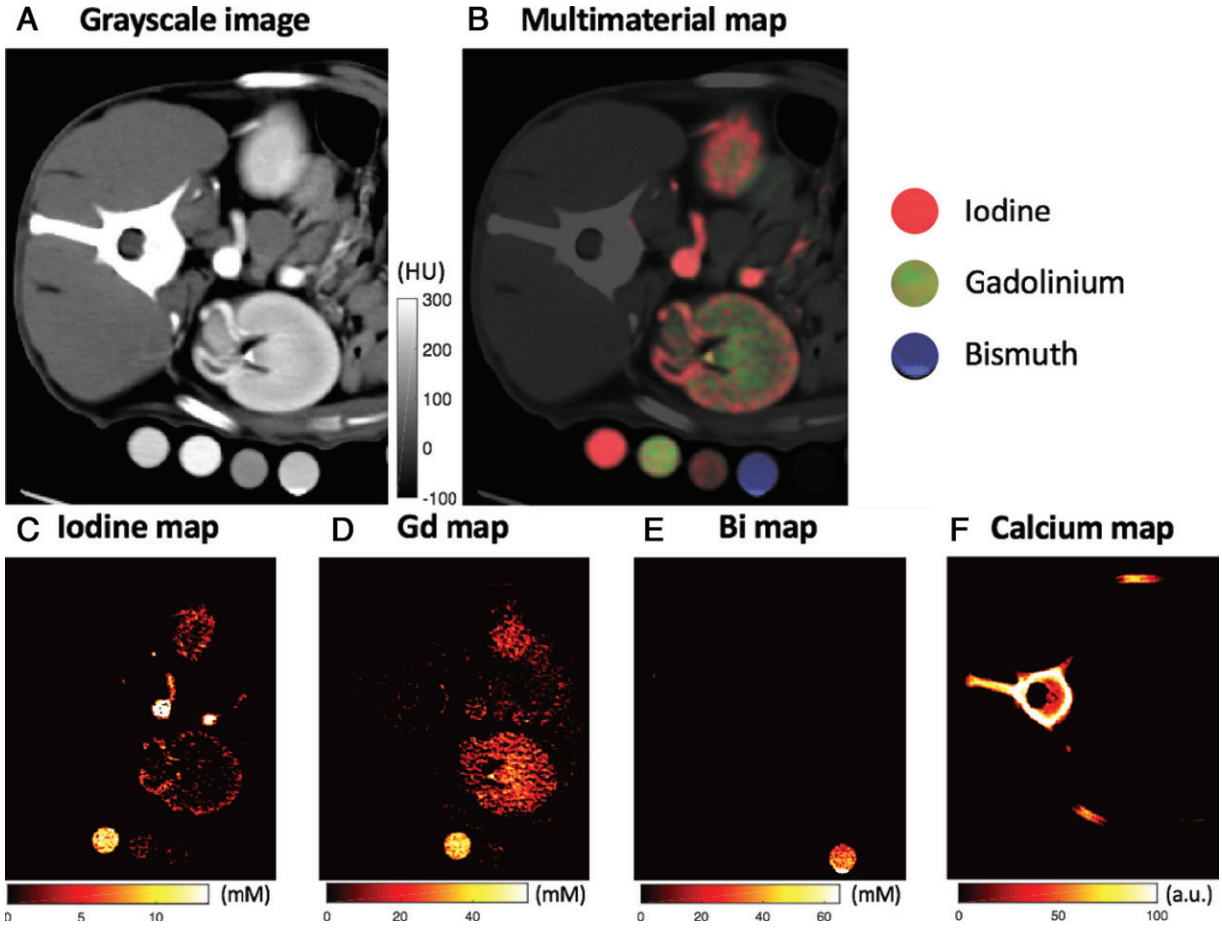

Figure 13: Example of in vivo multi k-edge material imaging of canine performed with photon-counting detector (PCD) CT. *A*, Grayscale PCD image reconstructed from all photons detected, regardless of their detected energy, at level of left pelvis demonstrates the dense contrast material in calibration vials, abdominal aorta, and kidney. No differentiation is possible between the different contrast agents with single-energy CT. *B*, PCD multimaterial map enables differentiation between iodine, gadolinium, and bismuth contrast agents. *C*, Iodine, *D*, gadolinium (*Gd*), *E*, bismuth (*Bi*), and, *F*, calcium material maps reveal calibration vials containing different contrast agents, with arterial corticomedullary iodine enhancement and venous nephrogenic and/or excretory enhancement within kidney. (Reprinted, with permission, from reference 49.)

EID images owing to their equal energy weighting of photons. However, equal weighting provides better CNR between soft tissues as well as between soft tissues and contrast agents. Gutjahr et al (4) have shown that a 140-kV PCD scan has iodine CNR similar to that on a 120-kV EID scan; Pourmorteza et al (75) showed good agreement between Hounsfield units on 120-kV EID and 140-kV PCD abdominal scans in humans. Furthermore, the inherent spectral information of photon-counting CT can be used to calculate virtual monoenergetic images and material concentration maps, which theoretically eliminate beam-hardening artifacts while still achieving the same CNR as optimal weighting (76). Symons et al (22) took advantage of this and obtained PCD scans of the head and neck at 140 kV, with CNRs comparable to that in a 120-kV EID image in a cohort of human volunteers. They reported less severe beam-hardening artifacts with PCD (Fig 18). Furthermore, they calculated iodine concentration maps and virtual monoenergetic images from photon-counting CT, which also showed less beam hardening. These were used to differentiate calcified plaques from the intravascular iodine in the carotid arteries (Fig 19).

Another way to reduce beam hardening is to use the high-energy portion of the PCD data. In an in vivo human brain study, Pourmorteza et al (21) showed that photon-counting CT images reconstructed from the high-energy photons were less contaminated by beam-hardening artifacts compared with the image reconstructed from all detected photons. However, this reduces tissue contrast (Figs 18, 20) (21,33,77). Dual-energy CT also allows for beam-hardening reduction by using material decomposition and by evaluating high monochromatic energy images. However, the performance of photon-counting CT is expected to be better owing to improved spectral separation (23).

Metal artifacts.—Metal artifacts are caused by multiple effects, including severe beam hardening. With conventional CT, prosthesis loosening may be mimicked by periprosthetic blackness caused by beam hardening, photon starvation, edge effects, and scatter (78). Photon-counting CT potentially allows for improved evaluation of prosthesis loosening due to reduced beam-hardening artifacts, lack of electronic

noise, and higher spatial resolution. Metal artifact reduction algorithms that rely on the multiple energy bins of photon-counting CT have been proposed (79). Figure 21 shows beam-hardening reduction in the first patient study obtained with a photon-counting CT prototype.

Blooming artifacts.—In addition to beam hardening, CT is also affected by blooming artifacts. These artifacts deteriorate visualization of the vessel lumen next to calcified plaques and of vasculature near bony structures and implanted stents, coils, and devices (81). Multienergy photon-counting CT has the potential to reduce blooming by means of improved spatial resolution and material decomposition. This is especially important in small stent evaluation, where two highly attenuating materials (iodine and stent metal) are present. Recent studies have shown the utility of high-spatial-resolution multienergy cardiovascular photon-counting CT in reducing blooming in human hearts (68) (Fig 15) and in coronary stents (69) (Fig 17).

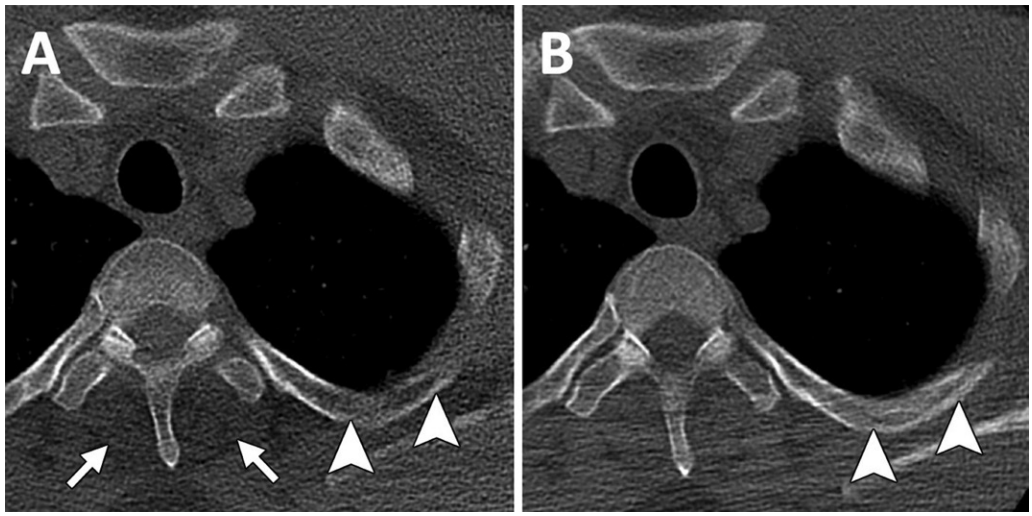

Figure 14: Effect of elimination of electronic noise. Example energy-integrating detector (EID) and photon-counting detector (PCD) CT images in 59-year-old man. *A*, EID image shows low-attenuation areas in paraspinal muscles (arrows) in lung apices due to beam hardening and electronic noise. Cortex of a left upper rib (arrowheads) appears eroded. *B*, PCD image at same level as *A* shows a more uniform appearance of the erector spinae muscles. Cortex of the upper left rib (arrowheads) is better visualized. Overall image noise is lower with PCD, as seen in the pectoral muscles. Images were acquired at identical settings and were reconstructed with similar algorithm and convolution kernels. (Reprinted, with permission, from reference 26.)

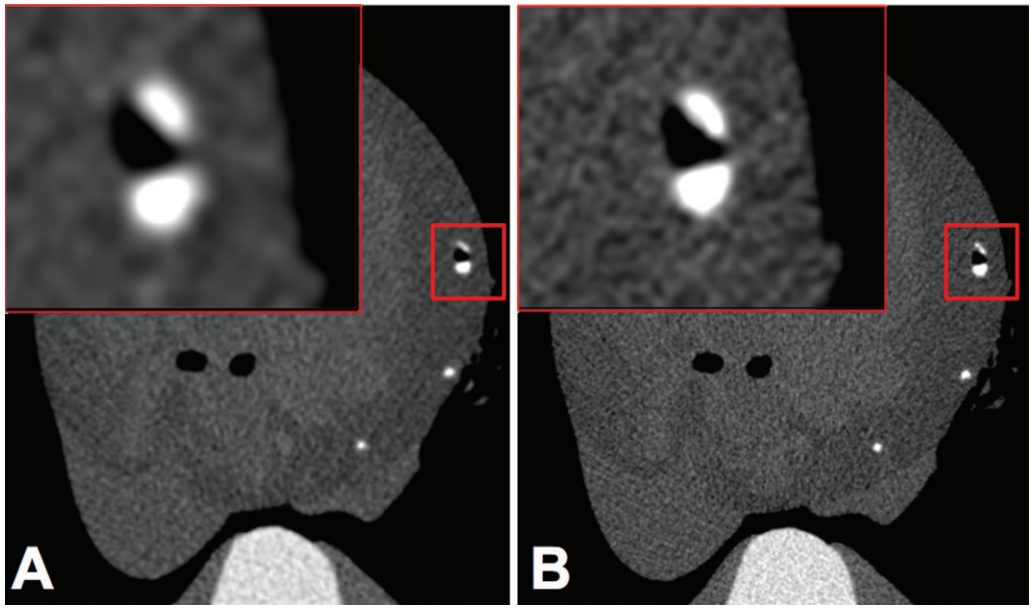

Figure 15: Reduction of the detector element size by half in photon-counting detector (PCD) reduced blooming of calcified plaques in this ex vivo human heart sample. Images were acquired at similar tube voltage, current, and focal spot size. *A*, PCD CT image acquired at standard resolution (macro mode) and, *B*, high-spatial-resolution (sharp mode) image obtained with prototype scanner (Siemens Healthineers, Forchheim, Germany). (Images are from National Institutes of Health [68].)

Contrast Agents

Photon-counting CT has the potential to improve CNRs, allowing for improved characterization of hypervascular lesions and feeding arteries of some neoplasms, better visualization of smaller vessels, and reduction of iodine load. Photon-counting CT provides a unique opportunity to use contrast agents other than iodine (including targeted imaging agents) and, potentially, multiple contrast agents, which can be imaged simultaneously with this type of scanner. Similar to dual-energy CT, it allows for removal of iodine from images, resulting in virtual noncontrast images.

Reduction of iodine load.—Although radiation dose reduction is important when scanning young patients, radiation exposure

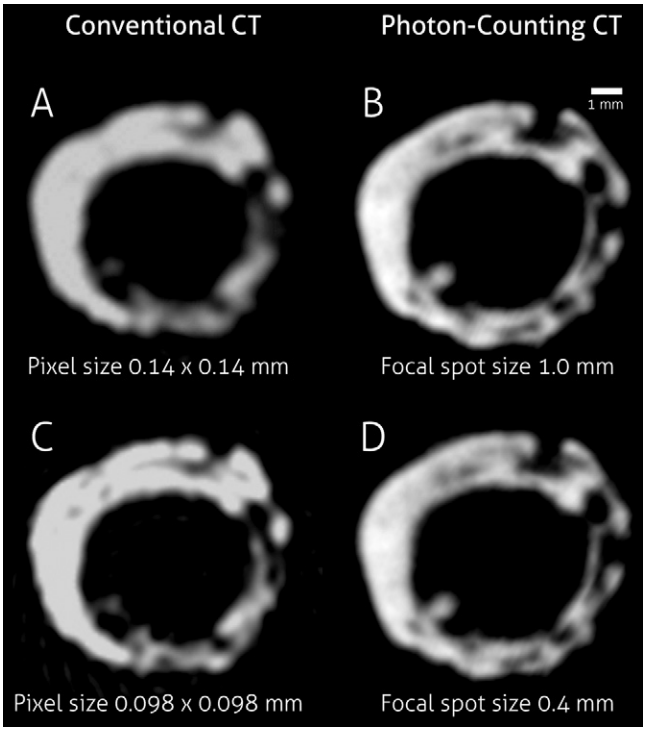

Figure 16: Images of ex vivo carotid artery cast in paraffin obtained with conventional clinical CT with 80 kVp and, *A*, normal resolution (0.14 × 0.14 mm^2 pixels) and, *C*, high spatial resolution (0.098 × 0.098 mm^2 pixels). For comparison, images were also acquired with a photon-counting silicon-strip detector module in a tabletop imaging setup, at 80 kVp, by using, *B*, normal focal spot size (focal spot size, 1.0 × 1.0 mm^2) and, *D*, small focal spot size (focal spot size, 0.4 × 0.4 mm^2). Image processing has been applied to remove ring artifacts. Note the high spatial resolution of the photon-counting CT images. (Image courtesy of Mats Danielsson, PhD, KTH Royal Institute of Technology, Stockholm, Sweden.)

concerns are lower in older patients. Because kidney function deteriorates with age, it may be of greater relevance to reduce contrast agent load in this population. Methods for reducing iodine load include reduction of tube voltage with conventional CT and use of low monochromatic images with dual-energy CT (82–84). Iodine CNRs are further improved with photon-counting CT because of the improved spectral separation and material decomposition. Multiple studies have shown that CNRs are better with PCDs compared with conventional EIDs. A study published by Yu and colleagues (33) showed that the CNR of iodine-based contrast material versus water increased by up to 25.5%. These improved iodine CNRs can be relevant for any application and can allow for reduction of iodine load. On the other hand, improved CNRs (with the same iodine load) may also facilitate iodine-specific applications, such as improved visualization of coronary arteries, assessment of subtle differences in myocardial enhancement in ischemia, and evaluation of endoleaks after endovascular repair of an aortic aneurysm with use of a stent-graft (81).

Alternative contrast agents.—Currently, the most commonly used contrast agents for CT are iodine (intravenous) and barium (oral). Only intravenous iodinated contrast agents can provide molar concentrations that are high enough to affect x-ray attenuation and tissue contrast. Gadolinium may serve as an alternative in patients with severe allergy to iodinated contrast agents, but substantially greater volumes would be required to achieve adequate molar concentrations and equal tissue contrast, at a much higher cost. Although dual-energy CT may enable the use of different contrast agents (85), spectral separation in dual-energy CT is not perfect, making the use of alternative agents challenging (23). Photon-counting CT has the potential to exploit high-atomic-number elements other than iodine, barium, and gadolinium as contrast agents. Examples include gold and platinum (86,87); xenon, bismuth, lutetium, tungsten, silver, and ytterbium could also be evaluated for use in photon-counting CT (88). Chen et al (55) showed that, with similar molar concentrations of gadolinium and iodine, the signal (in terms of squared signal difference–to-noise ratio normalized by skin dose) with gadolinium is three to 10 times higher than that with iodine. However, the clinically acceptable doses of gadolinium are lower compared with iodine doses.

Molecular imaging.—Molecular CT imaging that uses new types of targeted contrast agents (6,89) is among the exciting possibilities that may become a reality with use of photon-counting CT. In molecular CT, nanoparticles are labeled by atoms with high atomic numbers (contrast agents). These combined particles are larger than conventional contrast agents and are thus not filtered out by the kidneys. They remain in the cardiovascular system longer than 24 hours (86). Moreover, these nanoparticles carry more targeting molecules, which allow for target-specific imaging. With k-edge imaging, photon-counting CT enables identification of heavy elements. To date, most of the research has focused on nanoparticles labeled with gold (90,91). Concentrations of these heavy elements are too low to be detected with conventional CT. However, gold nanoparticles may be detected and quantified by using k-edge imaging, even in the presence of other contrast agents, such as iodine (43). This technique is of great clinical interest because nanoparticles can be targeted to specific cells or enzymes.

In oncology, molecular CT may aid in early cancer diagnosis by helping to quantify mass and size of small tumors and determine the distribution of contrast agents and/or particles (92,93). The ability to evaluate tumor behavior may result in more accurate tumor prognosis. In cardiovascular imaging, this method may improve characterization of atherosclerotic plaque composition (94). Clinical outcomes of atherosclerotic plaques depend not only on lumen narrowing, but also on plaque composition. Researchers have evaluated the ability of dual-energy CT to help differentiate between iodinated lumen and plaque characteristics such as calcifications, fibrous tissue, and fat. Results have shown that dual-energy CT can be used to differentiate iodine from calcium, but the differentiation between fibrous tissue and fat remains a challenge for this type of scanner (95). Materials such as iodine and calcium have large differences in effective atomic numbers, which makes them relatively easy to identify. However, fibrous and fatty tissues have much smaller differences in effective atomic numbers, making it more challenging to differentiate these materials with dual-energy CT (81). Photon-counting

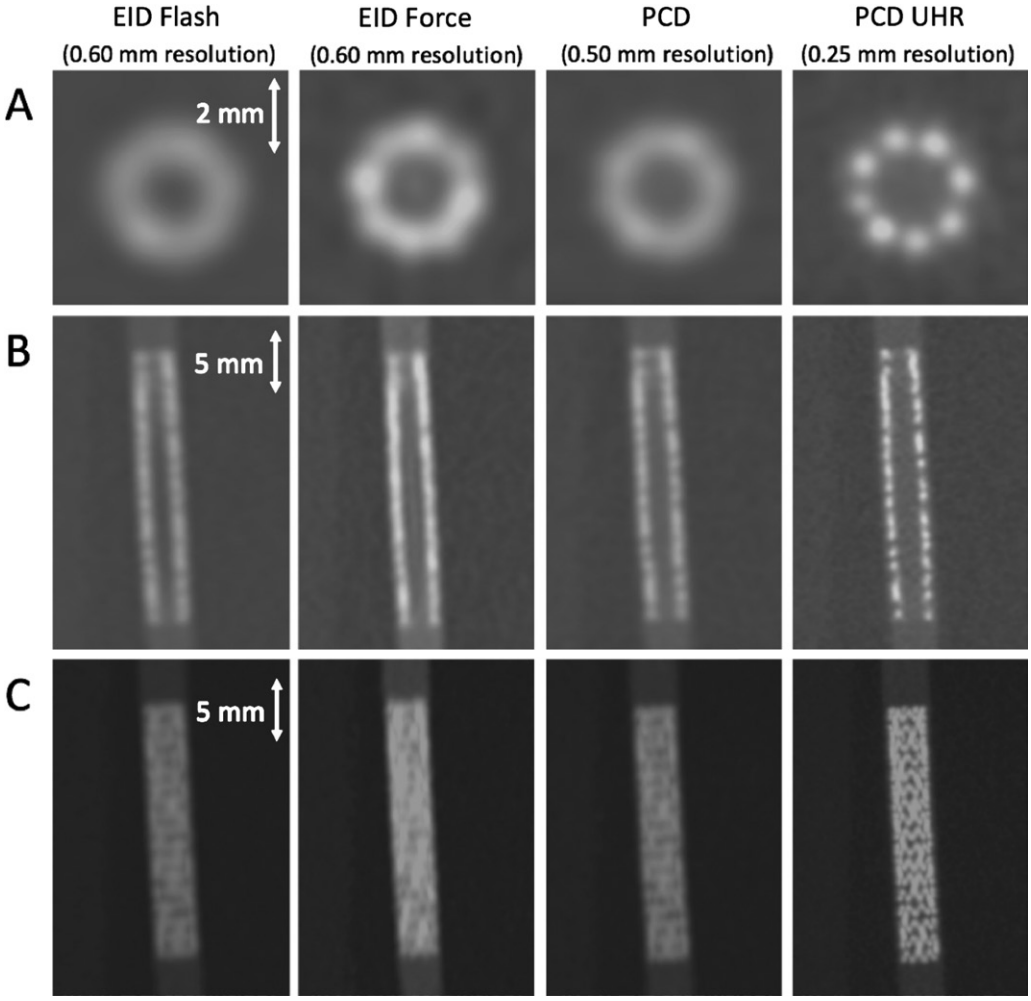

Figure 17: High-spatial-resolution dual-energy photon-counting detector (PCD) improves resolution and reduces blooming. *A*, Axial, *B*, coronal, and, *C*, coronal maximum intensity projections of scans of coronary stent (Synergy Monorail; Boston Scientific, Marlborough, Mass) made of a platinum chromium alloy, with nominal diameter of 2.75 mm, inside a coronary artery phantom consisting of plastic tubes filled with iodine-based contrast material diluted to approximate clinical concentrations (450 HU at 120 kV). Dual-energy energy-integrating detector (EID) images were acquired by using second- and third-generation dual-source CT systems (Somatom Flash and Somatom Force; Siemens Healthcare, Forchheim, Germany) at 0.60-mm isotropic voxel size. Radiation dose–matched PCD images were obtained with a prototype PCD system (Siemens Healthcare) at standard resolution (macro mode) and high resolution (*UHR*) (sharp mode). All images were reconstructed by using optimized convolution kernels and filtered backprojection algorithm. (Images from National Institutes of Health [69].)

CT is expected to be able to tackle this challenge due to the combination of improved spatial resolution, improved material decomposition, and the ability to use targeted contrast agents. Preclinical investigation results are promising, but it remains unclear whether the challenging task of adequate plaque characterization can be achieved at the temporal resolution needed to freeze cardiac motion (96).

Many challenges must be addressed before molecular CT can be used clinically. These include safety issues such as toxicity, stability, and clearance; functionality issues such as uniformity of nanoparticle size and particle concentrations; and signal detection (6). The agents also require regulatory approval before routine clinical use.

Simultaneous multi–contrast agent imaging.—Because photon-counting CT allows for k-edge imaging, which enables differentiation between multiple contrast agents, it may be possible to simultaneously administer different contrast agents and show their specific distribution, resulting in additional information. Administration of contrast agents such as iodine or gadolinium can be combined with administration of targeted nanoparticles (97). In addition, multiple nanoparticles targeted at different tissue types may be administered at the same time (6). This could help detect culprit coronary lesions. In addition to targeted nanoparticles, contrast agents such as iodine and/or barium and gadolinium may be combined. This implies that multiple contrast agents could be administered at different time points but imaging would be performed at a single time point (86). Noncontrast images could be reconstructed by removing the contrast agents from the images. The arterial phase could be evaluated by removing the contrast agent that was administered first, and the portal phase could be assessed by removing the second contrast agent (Fig 22). Muenzel et al (31) evaluated a colon phantom filled with iodine and a gadolinium-filled capsule simulating a polyp and concluded that contrast material maps helped clearly differentiate between iodine and gadolinium, with adequate contrast measurements (Fig 11). More recently, Symons and colleagues (48,49) evaluated simultaneous imaging in a canine model with orally administered bismuth and intravenously injected gadolinium and iodine. The prototype photon-counting CT system enabled the quantification of concentrations and simultaneous wash-in and washout kinetics of all contrast agents, as well as tissue enhancement of the heart and the kidney in a single acquisition (Figs 12, 13). Capturing multiple contrast phases in a single scan acquisition is theoretically possible for any multiphase CT protocol, including imaging of the liver, adrenal abnormalities, and aortic aneurysm. This method could reduce radiation doses because the patient

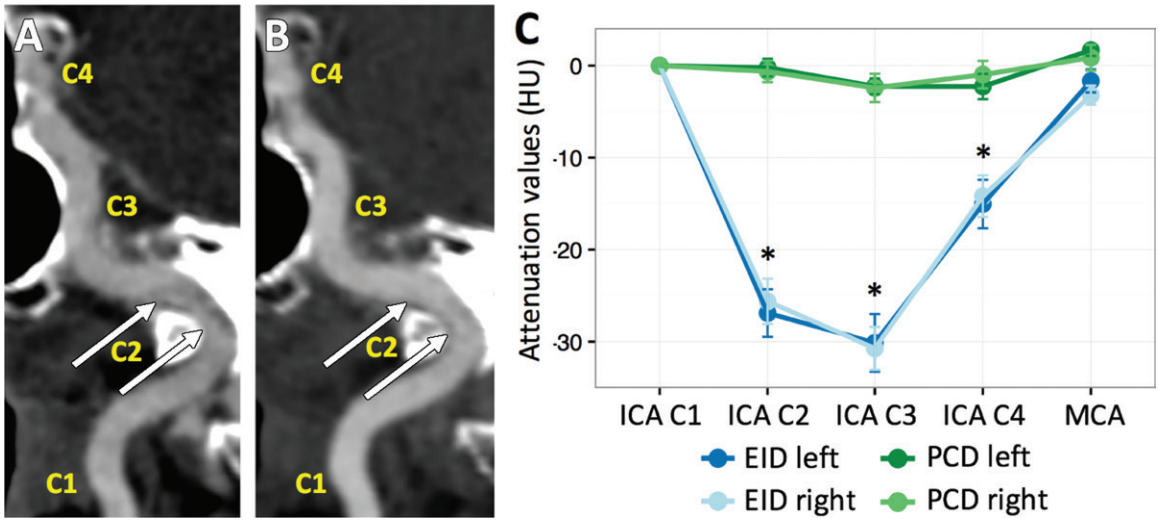

Figure 18: Beam hardening reduction in photon-counting detector (PCD) (140 kV) compared with energy-integrating detector (EID) (120 kV). *A*, EID image and, *B*, PCD image curved multiplanar reconstructions of internal carotid artery in 55-year-old woman. Artifactual areas of low attenuation within petrous segment of internal carotid artery (C2), which may be mistaken for pathologic condition, are seen on EID image but not on PCD image (arrows). *C*, Graph shows changes in Hounsfield units of iodine (means ± standard errors) in internal carotid artery (*ICA*) and middle cerebral artery (*MCA*) for 10 subjects. Hounsfield units are normalized to cervical ICA (C1) segment. Mean EID Hounsfield units in internal carotid artery segments C2, C3, and C4 were 26.3 HU, 30.4 HU, and 14.6 HU, respectively, which are lower than those in segment C1 ($P < .001$ for all). Mean PCD Hounsfield units, however, did not change significantly ($P > .05$ for all). (Images are from National Institutes of Health; reprinted, with permission, from reference 22.)

needs to be scanned only once instead of three times. Moreover, images from different phases would be matched perfectly, enabling the detection and characterization of small lesions. The technique could also improve patient throughput. The major disadvantage is that administration of two different contrast agents could cause image noise amplification, as more materials are separated by using a linear material decomposition algorithm.

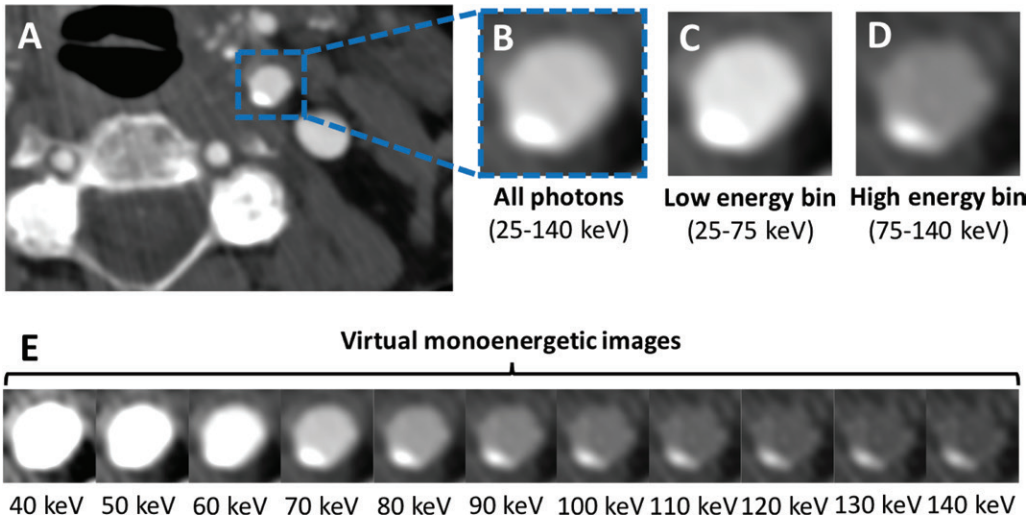

Figure 19: In vivo example of photon-counting detector (PCD) virtual monochromatic images of carotid plaque. *A*, Gray-scale PCD image reconstructed from all detected photons at level of proximal cervical internal carotid artery (segment C1) in 73-year-old woman demonstrates mild eccentric calcified plaque. *B*, Zoomed-in image of internal carotid artery segment C1 with corresponding, *C*, low- and, *D*, high-energy bin images. *E*, On the basis of the specific behavior of materials at different photon energies, images can be decomposed into their constituent materials (eg, iodine vs calcium) and virtual monoenergetic images can be reconstructed to facilitate plaque detection (window center: 145 HU, window width: 800 HU). (Reprinted, with permission, from reference 22.)

Virtual noncontrast CT.— Similar to dual-energy CT, iodine or other contrast agents can be detected and removed from the images acquired with photon-counting CT, resulting in virtual noncontrast CT images with perfect registration to the contrast-enhanced image (98). Noncontrast acquisition may be skipped when this technique becomes available. Photon-counting CT can result in more realistic virtual noncontrast images compared with dual-energy CT due to its improved spectral separation (23).

Quantitative Imaging

Pixel values in CT are currently expressed in Hounsfield units. These values could be quantitative estimates of the attenuation of the incident x-ray photons. However, defining an exact physical meaning of voxel values is not possible with conventional CT (6) because attenuation is energy-dependent and x-ray sources have a broad distribution of photon energies, depending on the protocol and, more importantly, the object being imaged. With

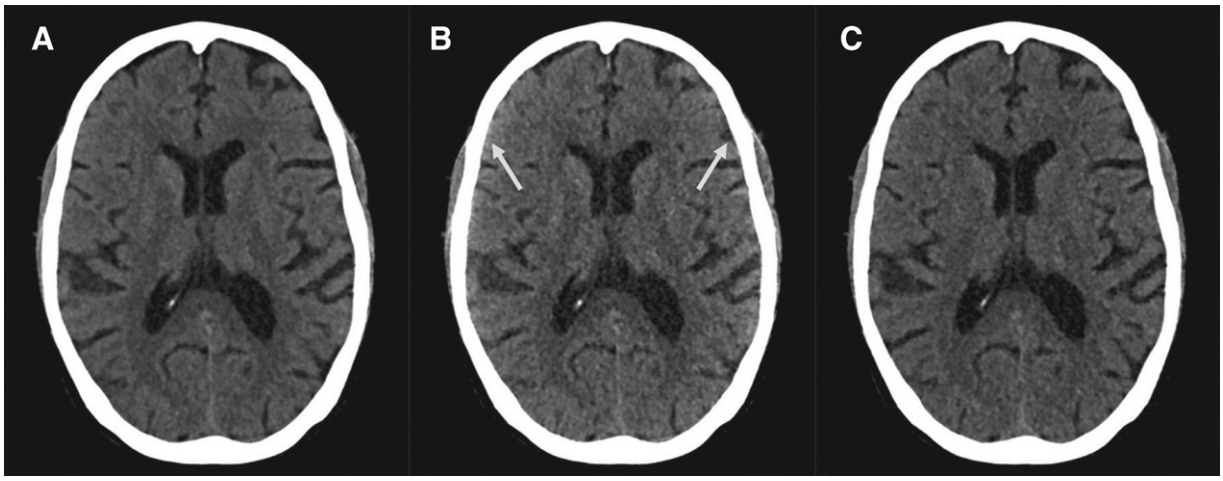

Figure 20: Beam hardening reduction in high-energy portion of photon-counting detector (PCD) image. Sample PCD images of low- and high-energy bins in 70-year-old woman (section thickness, 2 mm; increment, 2 mm; window center, 45 HU; window width, 80 HU). *A*, Axial PCD image reconstructed from all detected photons (22–120 keV) at level of basal ganglia. *B*, Axial PCD image reconstructed from low-energy bin image (22–52 keV) at same level as *A*. *C*, Axial PCD image reconstructed from high-energy bin image (52–120 keV) at same level as *A*. Image noise for both the low- and high-energy bins is higher than that of PCD image reconstructed from all detected photons because each bin contains only a subset of all detected photons. The low-energy bins provide good gray matter–white matter differentiation but are susceptible to beam hardening, which is best seen as an artifactual increase in attenuation of cortical gray matter and subarachnoid space (arrows). High-energy photons are less susceptible to beam hardening but have poorer gray matter–white matter differentiation. Image reconstructed from all photons is a trade-off between the good gray matter–white matter differentiation of the low-energy image and the lower beam-hardening artifacts of the high-energy images. (Images are from the National Institutes of Health; reprinted, with permission, from reference 21.)

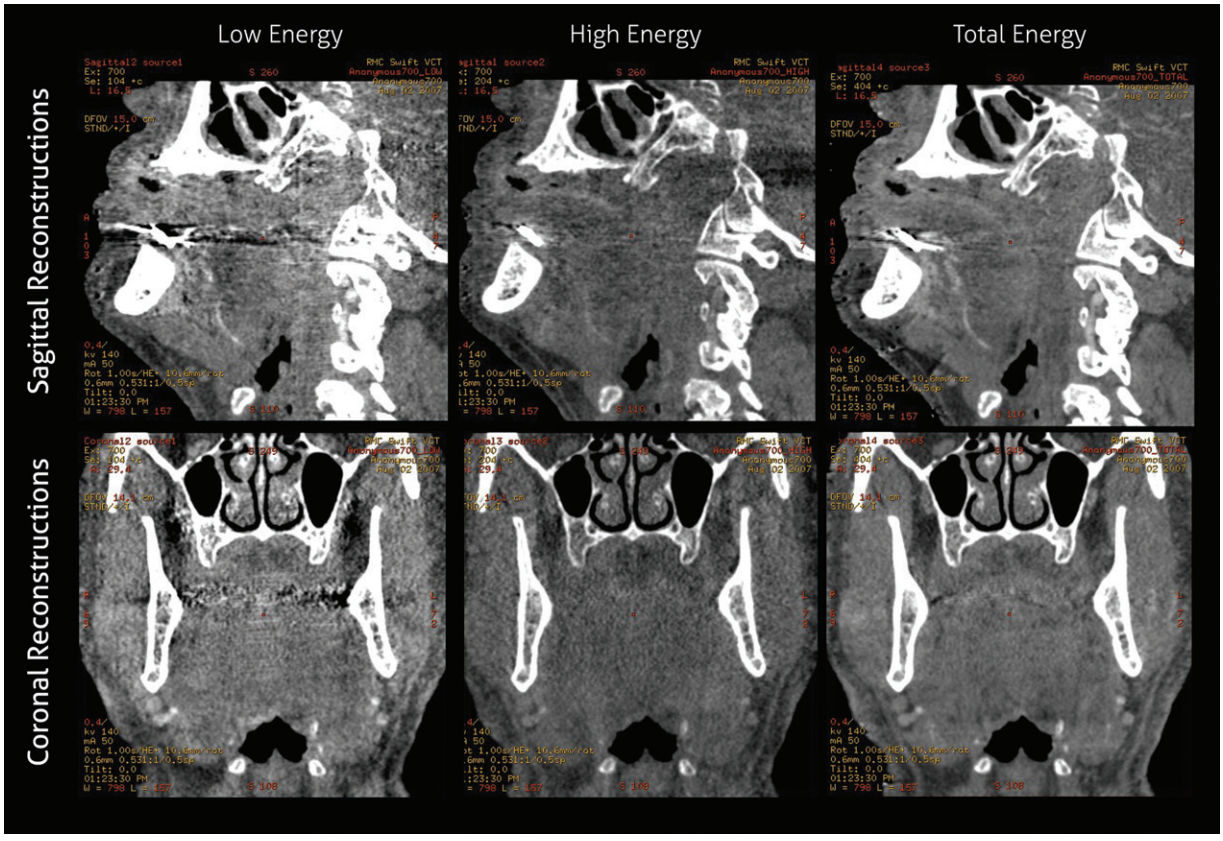

Figure 21: Images from first patient study with photon-counting CT, acquired with a prototype system (GE Healthcare, Chicago, Ill). Upper row shows sagittal images reconstructed at a low energy bin, high energy bin, and combined total energy, respectively. Lower row shows coronal images reconstructed at a low energy bin, high energy bin, and combined total energy, respectively. Note beam-hardening artifact reduction with the high energy bin. (Image courtesy of Ofer Benjaminov, MD, Rabin Medical Center, Israel, and Bob Senzig, MS, GE Healthcare.)

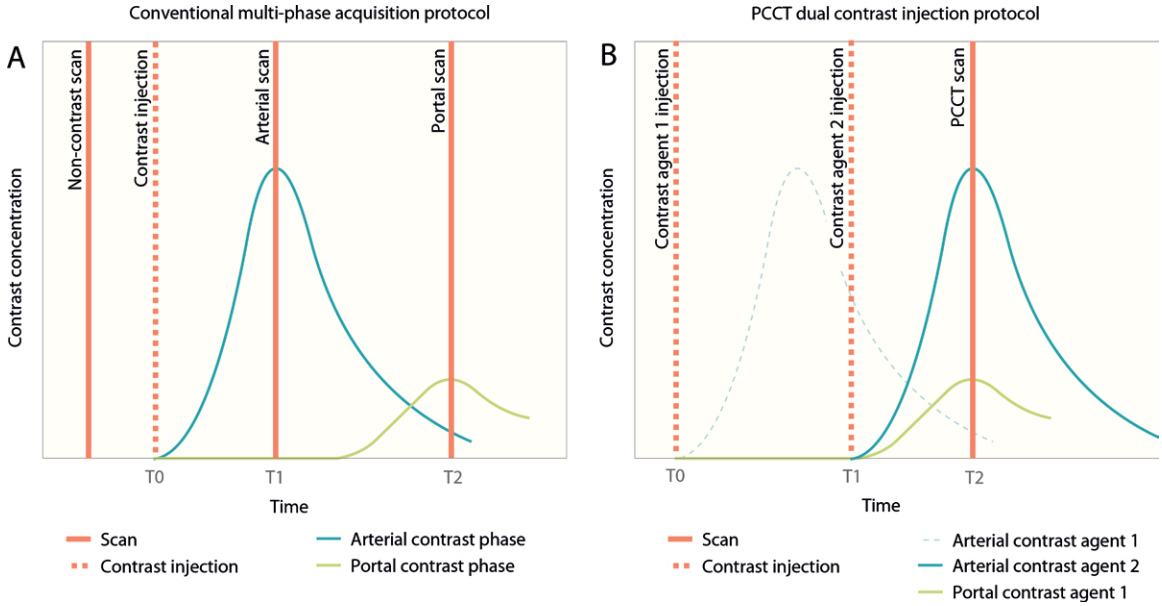

Figure 22: Dual contrast agent injection with photon-counting CT, as proposed by Muenzel et al (80). *A*, In conventional multiphase acquisition, a noncontrast scan is acquired first, followed by intravenous contrast agent injection. The second scan is obtained during arterial phase (T1), and a third scan is obtained during portal phase (T2). *B*, Dual contrast agent injection with photon-counting CT (*PCCT*) begins with intravenous administration of first contrast agent (T0, eg, iodine); after a specific period of time, a second contrast agent is administered (T1, eg, gadolinium). Subsequently, a single photon-counting CT scan is acquired when first contrast agent is in portal phase and second contrast agent is in arterial phase (T2). A virtual noncontrast scan can be reconstructed by removing both contrast agents, a portal phase scan can be reconstructed by removing the second contrast agent, and an arterial phase scan can be reconstructed by removing the first contrast agent. With this method, only one acquisition is needed instead of three.

photon-counting CT, on the other hand, we can measure the energy of every x-ray photon that hits the detector and determine fundamental physical properties of every voxel (34,43). Therefore, specific materials can be differentiated with photon-counting CT by using color-coded material-specific images (Figs 11, 12). Moreover, concentrations of certain materials, such as contrast agents and calcium, can be quantified. Photon-counting CT should allow for quantitative evaluation of bone mineral density and inflammation in gout, as well as the characterization of kidney stones (99). These functions are already possible with dual-energy CT, but quantification is expected to be more accurate with photon-counting CT. We anticipate improved perfusion imaging in quantitative photon-counting CT. With current CT systems, perfusion CT can be performed by acquiring a baseline scan followed by multiple target scans. After subtracting the baseline scan from the target scans, contrast enhancement within certain tissues can be calculated. The major disadvantage of this method is motion between the baseline scan and the target scans, which results in misregistration. Calculations are affected, resulting in inaccurate perfusion measurements (55). With conventional perfusion CT, a baseline scan is needed for subtraction. Because absolute concentrations can be quantified for every pixel with photon-counting CT, the baseline scan is not needed when using this technique (it should be zero in the baseline). This method can be valuable when assessing perfusion of multiple organs, including the brain, heart, liver, and lungs, and could also help evaluate perfusion of smaller structures such as the arterial wall (100). Moreover, multiple contrast agents could be used simultaneously for perfusion imaging, allowing for multiphase information in a single acquisition; this has been evaluated by Symons et al (48) in an occlusion-reperfusion canine model of the coronaries. In addition, lack of electronic noise in photon-counting CT results in more accurate and robust Hounsfield unit values, especially in low-dose acquisitions, as shown by Symons et al (25).

Conclusion

Photon-counting CT is a promising technique on the verge of becoming clinically feasible and has the potential to dramatically alter the clinical use of CT in the upcoming decades. By using energy-resolving detectors instead of EIDs, photon-counting CT systems are able to count individual incoming x-ray photons and measure their energy. Prototype systems tested so far are not perfect but have shown promising results. PCDs can reduce image noise substantially, can increase spatial resolution, and can use k-edge imaging to measure the concentration of specific elements. These technical advances will lead to a reduction of radiation doses at CT imaging by at least 30%–40%. The increased spatial resolution has already proven to be valuable in breast CT but is also expected to assist in CT of the temporal bone, chest, coronary and other arteries, head and neck, orthopedic trauma, and possibly other applications. Other advantages are potential reduction of beam-hardening artifacts and reduction of blooming artifacts, allowing for improved luminal vessel evaluation. Photon-counting CT has the potential to improve contrast with current iodinated contrast agents or reduce iodine load if clinically indicated. Furthermore, it provides opportunities to

use other contrast agents, such as gadolinium, gold, and platinum, which could be beneficial for patients with iodine allergies. Photon-counting CT may allow for molecular imaging with targeted nanoparticles, resulting in improved early cancer diagnosis and characterization of atherosclerotic plaque composition. We anticipate that multiple contrast agents can be administered and evaluated separately in a single photon-counting CT scan, allowing for multiphase scanning with a single acquisition. Finally, CT numbers produced by current CT scanners are affected by the acquisition protocol and surrounding anatomy. This will change with photon-counting CT, in which every pixel will give exact physical material and/or tissue information, allowing for more accurate characterization of tissues and enhanced perfusion imaging at reduced radiation dose levels.

Acknowledgments: We thank Peter Noël, PhD, from the Technical University of Munich, Germany; Ofer Benjaminov, MD, from Rabin Medical Center, Israel; Bob Senzig, MS, from GE Healthcare; Mats Danielsson, PhD, from KTH Royal Institute of Technology, Sweden; and Rolf Symons, MD, from the National Institutes of Health for providing figures.

Disclosures of Conflicts of Interest: **M.J.W.** Activities related to the present article: disclosed no relevant relationships. Activities not related to the present article: is on the speakers bureau at Philips Healthcare. Other relationships: disclosed no relevant relationships. **M.P.** Activities related to the present article: is a paid consultant for Prismatic Sensors; was previously employed by Prismatic Sensors; is a stockholder in Prismatic Sensors; has patents approved and pending, with assignee Prismatic Sensors. Activities not related to the present article: disclosed no relevant relationships. Other relationships: disclosed no relevant relationships. **A.P.** Activities related to the present article: received a collaborative research and development grant from Siemens Healthcare and the National Institutes of Health Clinical Center. Activities not related to the present article: disclosed no relevant relationships. Other relationships: has a patent invention disclosure pending. **N.J.P.** Activities related to the present article: is on the scientific advisory board for Prismatic Sensors; receives research support from Philips Healthcare and GE Healthcare. Activities not related to the present article: is on the scientific advisory board of Izotropic Imaging, RefleXion Medical, and NanoX Imaging. Other relationships: disclosed no relevant relationships. **D.F.** Activities related to the present article: disclosed no relevant relationships. Activities not related to the present article: received research support from Siemens Healthineers and GE Healthcare; is on the speakers bureau at Siemens Healthineers; has ownership interest in iSchemaView. Other relationships: disclosed no relevant relationships.

References

1. Kooiman J, Pasha SM, Zondag W, et al. Meta-analysis: serum creatinine changes following contrast enhanced CT imaging. Eur J Radiol 2012;81(10):2554–2561.
2. Alvarez RE, Macovski A. Energy-selective reconstructions in x-ray computerized tomography. Phys Med Biol 1976;21(5):733–744.
3. Krauss B, Grant KL, Schmidt BT, Flohr TG. The importance of spectral separation: an assessment of dual-energy spectral separation for quantitative ability and dose efficiency. Invest Radiol 2015;50(2):114–118.
4. Gutjahr R, Halaweish AF, Yu Z, et al. Human imaging with photon counting-based computed tomography at clinical dose levels: contrast-to-noise ratio and cadaver studies. Invest Radiol 2016;51(7):421–429.
5. Persson M, Huber B, Karlsson S, et al. Energy-resolved CT imaging with a photon-counting silicon-strip detector. Phys Med Biol 2014;59(22):6709–6727.
6. Taguchi K, Iwanczyk JS. Vision 20/20: single photon counting x-ray detectors in medical imaging. Med Phys 2013;40(10):100901.
7. Bornefalk H, Danielsson M. Photon-counting spectral computed tomography using silicon strip detectors: a feasibility study. Phys Med Biol 2010;55(7):1999–2022.
8. Xu C, Danielsson M, Bornefalk H. Evaluation of energy loss and charge sharing in cadmium telluride detectors for photon-counting computed tomography. IEEE Trans Nucl Sci 2011;58(3):614–625.
9. Shikhaliev PM, Fritz SG, Chapman JW. Photon counting multienergy x-ray imaging: effect of the characteristic x rays on detector performance. Med Phys 2009;36(11):5107–5119.
10. Michel T, Anton G, Böhnel M, et al. A fundamental method to determine the signal-to-noise ratio (SNR) and detective quantum efficiency (DQE) for a photon counting pixel detector. Nucl Instrum Methods Phys Res A 2006;568(2):799–802.
11. Xu J, Zbijewski W, Gang G, et al. Cascaded systems analysis of photon counting detectors. Med Phys 2014;41(10):101907.
12. Roessl E, Brendel B, Engel KJ, Schlomka JP, Thran A, Proksa R. Sensitivity of photon-counting based k-edge imaging in x-ray computed tomography. IEEE Trans Med Imaging 2011;30(9):1678–1690.
13. Kappler S, Henning A, Kreisler B, Schoeck F, Stierstorfer K, Flohr T. Photon counting CT at elevated x-ray tube currents: contrast stability, image noise and multi-energy performance. In: Whiting BR, Hoeschen C, eds. Proceedings of SPIE: medical imaging 2014—physics of medical imaging. Vol 9033. Bellingham, Wash: International Society for Optics and Photonics, 2014; 90331C.
14. Alvarez RE. Signal to noise ratio of energy selective x-ray photon counting systems with pileup. Med Phys 2014;41(11):111909.
15. Taguchi K, Zhang M, Frey EC, et al. Modeling the performance of a photon counting x-ray detector for CT: energy response and pulse pileup effects. Med Phys 2011;38(2):1089–1102.
16. Wang AS, Harrison D, Lobastov V, Tkaczyk JE. Pulse pileup statistics for energy discriminating photon counting x-ray detectors. Med Phys 2011;38(7):4265–4275.
17. Knoll GF. Radiation detection and measurement. 4th ed. Hoboken, NJ: Wiley, 2010.
18. Schmidt TG. Optimal "image-based" weighting for energy-resolved CT. Med Phys 2009;36(7):3018–3027.
19. Tapiovaara MJ, Wagner RF. SNR and DQE analysis of broad-spectrum x-ray imaging. Phys Med Biol 1985;30(6):519–529.
20. Shikhaliev PM. Beam hardening artefacts in computed tomography with photon counting, charge integrating and energy weighting detectors: a simulation study. Phys Med Biol 2005;50(24):5813–5827.
21. Pourmorteza A, Symons R, Reich DS, et al. Photon-counting CT of the brain: in vivo human results and image-quality assessment. AJNR Am J Neuroradiol 2017;38(12):2257–2263.
22. Symons R, Reich DS, Bagheri M, et al. Photon-counting computed tomography for vascular imaging of the head and neck: first in vivo human results. Invest Radiol 2018;53(3):135–142.
23. Leng S, Zhou W, Yu Z, et al. Spectral performance of a whole-body research photon counting detector CT: quantitative accuracy in derived image sets. Phys Med Biol 2017;62(17):7216–7232.
24. Faby S, Kuchenbecker S, Sawall S, et al. Performance of today's dual energy CT and future multi energy CT in virtual non-contrast imaging and in iodine quantification: a simulation study. Med Phys 2015;42(7):4349–4366.
25. Symons R, Cork TE, Sahbaee P, et al. Low-dose lung cancer screening with photon-counting CT: a feasibility study. Phys Med Biol 2017;62(1): 202–213.
26. Symons R, Pourmorteza A, Sandfort V, et al. Feasibility of dose-reduced chest CT with photon-counting detectors: initial results in humans. Radiology 2017;285(3):980–989.
27. Luhta R, Chappo M, Harwood B, Mattson R, Salk D, Vrettos C. A new 2D-tiled detector for multislice CT. In: Flynn MJ, Hsieh J, eds. Proceedings of SPIE: medical imaging 2006—physics of medical imaging. Vol 6142. Bellingham, Wash: International Society for Optics and Photonics, 2006; 61420U.
28. Symons R, Cork T, Folio L, Bluemke D, Pourmorteza A. WE-FG-207B-07: feasibility of low dose lung cancer screening with a whole-body photon counting CT—first human results. Med Phys 2016;43(6Part42):3835.
29. Pelc NJ, Edic P, Wang G. High dose efficiency CT system. NIH RePORT web site. https://projectreporter.nih.gov/project_info_description.cfm?aid=9388345&icde=40662306&ddparam=&ddvalue=&ddsub=&cr=1&csb=default&cs=ASC&pball. Accessed August 16, 2018.
30. Ronaldson JP, Zainon R, Scott NJ, et al. Toward quantifying the composition of soft tissues by spectral CT with Medipix3. Med Phys 2012;39(11):6847–6857.
31. Muenzel D, Bar-Ness D, Roessl E, et al. Spectral photon-counting CT: initial experience with dual-contrast agent k-edge colonography. Radiology 2017;283(3):723–728.
32. Si-Mohamed S, Bar-Ness D, Sigovan M, et al. Review of an initial experience with an experimental spectral photon-counting computed tomography system. Nucl Instrum Methods Phys Res A 2017;873(Suppl C):27–35.
33. Yu Z, Leng S, Jorgensen SM, et al. Evaluation of conventional imaging performance in a research whole-body CT system with a photon-counting detector array. Phys Med Biol 2016;61(4):1572–1595.
34. Schlomka JP, Roessl E, Dorscheid R, et al. Experimental feasibility of multi-energy photon-counting k-edge imaging in pre-clinical computed tomography. Phys Med Biol 2008;53(15):4031–4047.
35. Szeles C, Soldner SA, Vydrin S, Graves J, Bale DS. CdZnTe semiconductor detectors for spectroscopic x-ray imaging. IEEE Trans Nucl Sci 2008;55(1):572–582.

36. Barber WC, Wessel JC, Nygard E, et al. High flux energy-resolved photon-counting x-ray imaging arrays with CdTe and CdZnTe for clinical CT. Presented at the 2013 3rd International Conference on Advancements in Nuclear Instrumentation, Measurement Methods and Their Applications (ANIMMA), Marseille, France, June 23–27, 2013.
37. Leng S, Yu Z, Halaweish A, et al. Dose-efficient ultrahigh-resolution scan mode using a photon counting detector computed tomography system. J Med Imaging (Bellingham) 2016;3(4):043504.
38. Baek J, Pineda AR, Pelc NJ. To bin or not to bin? The effect of CT system limiting resolution on noise and detectability. Phys Med Biol 2013;58(5):1433–1446.
39. Pourmorteza A, Symons R, Schöck F, et al. Image quality assessment and dose-efficiency of quarter-millimeter photon-counting CT of humans: first in vivo experience [abstr]. In: Radiological Society of North America scientific assembly and annual meeting program. Oak Brook, Ill: Radiological Society of North America, 2017; 101.
40. Rajbhandary PL, Hsieh SS, Pelc NJ. Effect of spatio-energy correlation in PCD due to charge sharing, scatter, and secondary photons. In: Flohr TG, Lo JY, Gilat Schmidt T, eds. Proceedings of SPIE: medical imaging 2017—physics of medical imaging. Vol 10132. Bellingham, Wash: International Society for Optics and Photonics, 2017; 101320V.
41. Giersch J, Niederlöhner D, Anton G. The influence of energy weighting on x-ray imaging quality. Nucl Instrum Methods Phys Res A 2004;531(1-2):68–74.
42. Schmidt TG. CT energy weighting in the presence of scatter and limited energy resolution. Med Phys 2010;37(3):1056–1067.
43. Roessl E, Proksa R. K-edge imaging in x-ray computed tomography using multi-bin photon counting detectors. Phys Med Biol 2007;52(15):4679–4696.
44. Alvarez RE. Dimensionality and noise in energy selective x-ray imaging. Med Phys 2013;40(11):111909.
45. Yu L, Christner JA, Leng S, Wang J, Fletcher JG, McCollough CH. Virtual monochromatic imaging in dual-source dual-energy CT: radiation dose and image quality. Med Phys 2011;38(12):6371–6379.
46. Johnson TR, Krauss B, Sedlmair M, et al. Material differentiation by dual energy CT: initial experience. Eur Radiol 2007;17(6):1510–1517.
47. Lakshmanan M, Symons R, Cork T, et al. WE-FG-207B-01: best in physics (imaging): abdominal CT with three k-edge contrast materials using a whole-body photon-counting scanner: initial results of a large animal experiment. Med Phys 2016;43(6Part42):3834.
48. Symons R, Cork TE, Lakshmanan MN, et al. Dual-contrast agent photon-counting computed tomography of the heart: initial experience. Int J Cardiovasc Imaging 2017;33(8):1253–1261.
49. Symons R, Krauss B, Sahbaee P, et al. Photon-counting CT for simultaneous imaging of multiple contrast agents in the abdomen: an in vivo study. Med Phys 2017;44(10):5120–5127.
50. Bornefalk H. Synthetic Hounsfield units from spectral CT data. Phys Med Biol 2012;57(7):N83–N87.
51. Shikhaliev PM. Computed tomography with energy-resolved detection: a feasibility study. Phys Med Biol 2008;53(5):1475–1495.
52. Liu X, Yu L, Primak AN, McCollough CH. Quantitative imaging of element composition and mass fraction using dual-energy CT: three-material decomposition. Med Phys 2009;36(5):1602–1609.
53. Yveborg M, Danielsson M, Bornefalk H. Theoretical comparison of a dual energy system and photon counting silicon detector used for material quantification in spectral CT. IEEE Trans Med Imaging 2015;34(3):796–806.
54. Bornefalk H, Persson M. Theoretical comparison of the iodine quantification accuracy of two spectral CT technologies. IEEE Trans Med Imaging 2014;33(2):556–565.
55. Chen H, Xu C, Persson M, Danielsson M. Optimization of beam quality for photon-counting spectral computed tomography in head imaging: simulation study. J Med Imaging (Bellingham) 2015;2(4):043504.
56. Berrington de González A, Mahesh M, Kim KP, et al. Projected cancer risks from computed tomographic scans performed in the United States in 2007. Arch Intern Med 2009;169(22):2071–2077.
57. Brenner DJ. Minimising medically unwarranted computed tomography scans. Ann ICRP 2012;41(3-4):161–169.
58. den Harder AM, Willemink MJ, de Jong PA, et al. New horizons in cardiac CT. Clin Radiol 2016;71(8):758–767.
59. McMillan K, Bostani M, Cagnon CH, et al. Estimating patient dose from CT exams that use automatic exposure control: development and validation of methods to accurately estimate tube current values. Med Phys 2017;44(8):4262–4275.
60. Willemink MJ, de Jong PA, Leiner T, et al. Iterative reconstruction techniques for computed tomography Part 1: technical principles. Eur Radiol 2013;23(6):1623–1631.
61. Kappler S, Hannemann T, Kraft E, et al. First results from a hybrid prototype CT scanner for exploring benefits of quantum-counting in clinical CT. In: Pelc NJ, Nishikawa RM, Whiting BR, eds. Proceedings of SPIE: medical imaging 2012—physics of medical imaging. Vol 8313. Bellingham, Wash: International Society for Optics and Photonics, 2012; 83130X.
62. Rößler AC, Kalender W, Kolditz D, et al. Performance of photon-counting breast computed tomography, digital mammography, and digital breast tomosynthesis in evaluating breast specimens. Acad Radiol 2017;24(2):184–190.
63. Shikhaliev PM. Soft tissue imaging with photon counting spectroscopic CT. Phys Med Biol 2015;60(6):2453–2474.
64. Leng S, Yu Z, Halaweish A, et al. A high-resolution imaging technique using a whole-body, research photon counting detector CT system. In: Kontos D, Flohr TG, eds. Proceedings of SPIE: medical imaging 2016—physics of medical imaging. Vol 9783. Bellingham, Wash: International Society for Optics and Photonics, 2016; 97831I.
65. Leng S, Gutjahr R, Ferrero A, et al. Ultra-high spatial resolution, multi-energy CT using photon counting detector technology. In: Flohr TG, Lo JY, Gilat Schmidt T, eds. Proceedings of SPIE: medical imaging 2017—physics of medical imaging. Vol 10132. Bellingham, Wash: International Society for Optics and Photonics, 2017; 101320Y.
66. Zhou W, Montoya J, Gutjahr R, et al. Lung nodule volume quantification and shape differentiation with an ultra-high resolution technique on a photon counting detector CT system. Proc SPIE Int Soc Opt Eng 2017 Feb 11;10132.
67. Taylor AJ, Cerqueira M, Hodgson JM, et al. ACCF/SCCT/ACR/AHA/ASE/ASNC/NASCI/SCAI/SCMR 2010 appropriate use criteria for cardiac computed tomography: a report of the American College of Cardiology Foundation Appropriate Use Criteria Task Force, the Society of Cardiovascular Computed Tomography, the American College of Radiology, the American Heart Association, the American Society of Echocardiography, the American Society of Nuclear Cardiology, the North American Society for Cardiovascular Imaging, the Society for Cardiovascular Angiography and Interventions, and the Society for Cardiovascular Magnetic Resonance. Circulation 2010;122(21):e525–e555.
68. Sandfort V, Symons R, Cork TE, Bluemke DA, Pourmorteza A. 250 micron resolution photon-counting CT: potential for improved imaging of calcified coronary artery stenoses [abstr]. In: Radiological Society of North America scientific assembly and annual meeting program. Oak Brook, Ill: Radiological Society of North America, 2017; 139.
69. Symons R, Roosen J, Debruecker Y, et al. Spectral ultra-high resolution coronary stent imaging with photon-counting CT: initial experience [abstr]. In: Radiological Society of North America scientific assembly and annual meeting program. Oak Brook, Ill: Radiological Society of North America, 2017; 101.
70. Guggenberger R, Gnannt R, Hodler J, et al. Diagnostic performance of dual-energy CT for the detection of traumatic bone marrow lesions in the ankle: comparison with MR imaging. Radiology 2012;264(1):164–173.
71. Kellock TT, Nicolaou S, Kim SSY, et al. Detection of bone marrow edema in nondisplaced hip fractures: utility of a virtual noncalcium dual-energy CT application. Radiology 2017;284(3):798–805.
72. Pache G, Krauss B, Strohm P, et al. Dual-energy CT virtual noncalcium technique: detecting posttraumatic bone marrow lesions—feasibility study. Radiology 2010;256(2):617–624.
73. Reddy T, McLaughlin PD, Mallinson PI, et al. Detection of occult, undisplaced hip fractures with a dual-energy CT algorithm targeted to detection of bone marrow edema. Emerg Radiol 2015;22(1):25–29.
74. Kuno H, Onaya H, Iwata R, et al. Evaluation of cartilage invasion by laryngeal and hypopharyngeal squamous cell carcinoma with dual-energy CT. Radiology 2012;265(2):488–496.
75. Pourmorteza A, Symons R, Sandfort V, et al. Abdominal imaging with contrast-enhanced photon-counting CT: first human experience. Radiology 2016;279(1):239–245.
76. Alvarez RE. Near optimal energy selective x-ray imaging system performance with simple detectors. Med Phys 2010;37(2):822–841.
77. Yu Z, Leng S, Jorgensen SM, et al. Initial results from a prototype whole-body photon-counting computed tomography system. In: Hoeschen C, Kontos D, eds. Proceedings of SPIE: medical imaging 2015—physics of medical imaging. Vol 9412. Bellingham, Wash: International Society for Optics and Photonics, 2015; 94120W.
78. Boas FE, Fleischmann D. Evaluation of two iterative techniques for reducing metal artifacts in computed tomography. Radiology 2011;259(3):894–902.
79. Nasirudin RA, Mei K, Penchev P, et al. Reduction of metal artifact in single photon-counting computed tomography by spectral-driven iterative reconstruction technique. PLoS One 2015;10(5):e0124831.
80. Muenzel D, Proksa R, Daerr H, et al. Photon counting CT of the liver with dual-contrast enhancement. In: Kontos D, Flohr TG, eds. Proceedings of SPIE: medical imaging 2016—physics of medical imaging. Vol 9783. Bellingham, Wash: International Society for Optics and Photonics, 2016; 97835N.

81. Wang AS, Hsieh SS, Pelc NJ. Dual-energy and multienergy techniques in vascular imaging. In: Saveden C, Rudin S, eds. Cardiovascular and neuromuscular imaging: physics and technology. Boca Raton, Fla: CRC, 2015; 191–202.
82. Dong J, Wang X, Jiang X, et al. Low-contrast agent dose dual-energy CT monochromatic imaging in pulmonary angiography versus routine CT. J Comput Assist Tomogr 2013;37(4):618–625.
83. Lu GM, Wu SY, Yeh BM, Zhang LJ. Dual-energy computed tomography in pulmonary embolism. Br J Radiol 2010;83(992):707–718.
84. Machida H, Tanaka I, Fukui R, et al. Dual-energy spectral CT: various clinical vascular applications. RadioGraphics 2016;36(4):1215–1232.
85. Mongan J, Rathnayake S, Fu Y, et al. In vivo differentiation of complementary contrast media at dual-energy CT. Radiology 2012;265(1):267–272.
86. Fornaro J, Leschka S, Hibbeln D, et al. Dual- and multi-energy CT: approach to functional imaging. Insights Imaging 2011;2(2):149–159.
87. Müllner M, Schlattl H, Hoeschen C, Dietrich O. Feasibility of spectral CT imaging for the detection of liver lesions with gold-based contrast agents: a simulation study. Phys Med 2015;31(8):875–881.
88. Yeh BM, FitzGerald PF, Edic PM, et al. Opportunities for new CT contrast agents to maximize the diagnostic potential of emerging spectral CT technologies. Adv Drug Deliv Rev 2017;113:201–222.
89. Jaffer FA, Weissleder R. Seeing within: molecular imaging of the cardiovascular system. Circ Res 2004;94(4):433–445.
90. Cormode DP, Skajaa T, Fayad ZA, Mulder WJ. Nanotechnology in medical imaging: probe design and applications. Arterioscler Thromb Vasc Biol 2009;29(7):992–1000.
91. Si-Mohamed S, Cormode DP, Bar-Ness D, et al. Evaluation of spectral photon counting computed tomography k-edge imaging for determination of gold nanoparticle biodistribution in vivo. Nanoscale 2017;9(46):18246–18257.
92. Barber WC, Wessel JC, Nygard E, Iwanczyk JS. Energy dispersive CdTe and CdZnTe detectors for spectral clinical CT and NDT applications. Nucl Instrum Methods Phys Res A 2015;784:531–537.
93. Meng B, Cong W, Xi Y, De Man B, Yang J, Wang G. Model and reconstruction of a k-edge contrast agent distribution with an x-ray photon-counting detector. Opt Express 2017;25(8):9378–9392.
94. Cormode DP, Roessl E, Thran A, et al. Atherosclerotic plaque composition: analysis with multicolor CT and targeted gold nanoparticles. Radiology 2010;256(3):774–782.
95. Barreto M, Schoenhagen P, Nair A, et al. Potential of dual-energy computed tomography to characterize atherosclerotic plaque: ex vivo assessment of human coronary arteries in comparison to histology. J Cardiovasc Comput Tomogr 2008;2(4):234–242.
96. Schirra CO, Brendel B, Anastasio MA, Roessl E. Spectral CT: a technology primer for contrast agent development. Contrast Media Mol Imaging 2014;9(1):62–70.
97. Cormode DP, Si-Mohamed S, Bar-Ness D, et al. Multicolor spectral photon-counting computed tomography: in vivo dual contrast imaging with a high count rate scanner. Sci Rep 2017;7(1):4784.
98. Iwanczyk JS, Nygård E, Meirav O, et al. Photon counting energy dispersive detector arrays for x-ray imaging. IEEE Trans Nucl Sci 2009;56(3):535–542.
99. Ferrero A, Gutjahr R, Henning A, et al. Renal stone characterization using high resolution imaging mode on a photon counting detector CT system. In: Flohr TG, Lo JY, Gilat Schmidt T, eds. Proceedings of SPIE: medical imaging 2017—physics of medical imaging. Vol 10132. Bellingham, Wash: International Society for Optics and Photonics, 2017; 101323J.
100. Jorgensen SM, Korinek MJ, Vercnocke AJ, et al. Arterial wall perfusion measured with photon counting spectral x-ray CT. In: Stock SR, Müller B, Wang G, eds. Proceedings of SPIE: optical engineering 2016—developments in x-ray tomography X. Vol 9967. Bellingham, Wash: International Society for Optics and Photonics, 2016; 99670B.